Development and application of observable response indicators for design of an effective ozone and fine particle pollution control strategy in China

Jia Xing[1,2], Dian Ding[1,2], Shuxiao Wang[1,2,*], Zhaoxin Dong[1,2], James T. Kelly[3], Carey Jang[3], Yun Zhu[4], Jiming Hao[1,2]

[1] State Key Joint Laboratory of Environmental Simulation and Pollution Control, School of Environment, Tsinghua University, Beijing 100084, China

[2] State Environmental Protection Key Laboratory of Sources and Control of Air Pollution Complex, Beijing 100084, China

[3] Office of Air Quality Planning and Standards, U.S. Environmental Protection Agency, Research Triangle Park, NC 27711, USA

[4] College of Environmental Science & Engineering, South China University of Technology, Guangzhou Higher Education Mega Center, Guangzhou, China

[*]Corresponding Author: Shuxiao Wang (email: shxwang@tsinghua.edu.cn; phone: +86-10-62771466; fax: +86-10-62773650)

Abstract

Designing effective control policies requires efficient quantification of the nonlinear response of air pollution to emissions. However, neither the current observable indicators nor the current indicators based on response-surface modeling (RSM) can fulfill this requirement. Therefore, this study developed new observable RSM-based indicators and applied them to ambient fine particle ($PM_{2.5}$) and ozone (O_3) pollution control in China. The performance of these observable indicators in predicting O_3 and $PM_{2.5}$ chemistry was compared with that of the current RSM-based indicators. H_2O_2×HCHO/NO_2 and total ammonia ratio, which exhibited the best performance among indicators, were proposed as new observable O_3- and $PM_{2.5}$-chemistry indicators, respectively. Strong correlations between RSM-based and traditional observable indicators suggested that a combination of ambient concentrations of certain chemical species can serve as an indicator to approximately quantify the response of O_3 and $PM_{2.5}$ to changes in precursor

emissions. The observable RSM-based indicator for O_3 (observable peak ratio) effectively captured the strong NO_x-saturated regime in January and the NO_x-limited regime in July, as well as the strong NO_x-saturated regime in northern and eastern China and their key regions, including the Yangtze River Delta and Pearl River Delta. The observable RSM-based indicator for $PM_{2.5}$ (observable flex ratio) also captured strong NH_3-poor condition in January and NH_3-rich condition in April and July, as well as NH_3-rich in northern and eastern China and the Sichuan Basin. Moreover, analysis of these newly developed observable response indicators suggested that the simultaneous control of NH_3 and NO_x emissions produces greater benefits in provinces with higher $PM_{2.5}$ exposure by up to 1.2 μg m^{-3} $PM_{2.5}$ per 10 % NH_3 reduction compared with NO_x control only. Control of volatile organic compound (VOC) emissions by as much as 40 % of NO_x controls is necessary to obtain the co-benefits of reducing both O_3 and $PM_{2.5}$ exposure at the national level when controlling NO_x emissions. However, the VOC-to-NO_x ratio required to maintain benefits varies significantly from 0 to 1.2 in different provinces, suggesting that a more localized control strategy should be designed for each province.

Keywords: nonlinear response, precursor emissions, response surface model, ozone, $PM_{2.5}$, indicator

1. Introduction

Air pollution has attracted great attention because of its harmful effects on human health (Cohen et al., 2017), climate (Myhre et al., 2013), agriculture and ecosystems (Fuhrer et al., 2016), and visibility (Friedlander et al., 1977). In particular, ambient fine particles ($PM_{2.5}$) and ozone (O_3) are among the top risk factors for global mortality (Forouzanfar et al., 2015; Cohen et al., 2017) and have increased the need to effectively control anthropogenic sources in order to reduce the ambient concentrations of $PM_{2.5}$ and O_3 (Wang et al., 2017). The challenge is that the dominant contributions to ambient $PM_{2.5}$ and O_3 arise from a series of chemical reactions among precursors, including sulfur dioxide (SO_2), nitrogen oxides (NO_x), ammonia (NH_3) and volatile organic compounds (VOCs) (Seinfeld and Pandis, 2012). The complexity of the chemical reactions and pathways associated with variations in meteorological conditions and precursor levels results in strong nonlinear responses of $PM_{2.5}$ and O_3 to their precursor emission changes (West et al., 1999; Hakami et al., 2004; Cohan et la., 2005; Pun et al., 2007; Megaritis et al., 2013). Such nonlinearity issues are a major challenge for policy-makers to design an effective control strategy.

Chemical species in the atmosphere are often highly correlated with one another, since their concentrations are affected by common atmospheric physical processes (e.g., mixing and transport) and chemical reactions. Concentrations of pollutants such as O_3 and $PM_{2.5}$ are typically determined based on the ambient levels of their gaseous precursors, implying that O_3 and $PM_{2.5}$ chemistry can be identified through a combination of concentrations of some of their related chemical species (i.e., indicators). The empirical kinetic modeling approach (EKMA) developed by the U.S. EPA quantifies the relationships of O_3 with its precursor concentrations based on O_3 chemistry (Freas et al., 1978; Gipson et al., 1981). The EKMA plot can aid inference of control strategy effectiveness (e.g., NO_x or VOC control) according to VOC-to-NO_x ratios. Several studies have developed "observable" indicators by relating O_3 to reactive

nitrogen concentrations and species related to atmospheric oxidation. Such indicators include NO_y, H_2O_2/HNO_3, $HCHO/NO_2$ and $H_2O_2/(O_3+NO_2)$ (Milford et al., 1994; Sillman, 1995; Tonnesen and Dennis, 2000; Sillman and He, 2002), which can be used to identify NOx-saturated or -limited regimes. The O_3 indicators can be derived from surface-monitoring observations (Peng et al., 2006), modeling simulations (Wang et al., 2010), or even satellite retrievals (Jin et al., 2017; Sun et al., 2018), and then examined using three-dimensional chemical transport models (CTMs) (Jiménez et al., 2004; Zhang et al., 2009; Liu et al., 2010; Ye et al., 2016). Regarding $PM_{2.5}$ chemistry (more specifically for inorganic $PM_{2.5}$ sensitivities to NH_3 and NO_x), indicators such as the degree of sulfate neutralization (DSN), gas ratio (GR), and adjusted gas ratio (AdjGR) have been developed (defined in Text S1) to identify NH_3-poor or -rich conditions (Ansari and Pandis, 1998; Takahama et al., 2004; Pinder et al., 2008; Dennis et al., 2008). The indicator-based method can be efficient in determining the chemical regime in the current scenarios and in qualitatively estimating O_3 and $PM_{2.5}$ sensitivities to small perturbations in precursor emissions or ambient concentrations without involving complex CTMs. However, traditional indicator methods are unable to quantify the extent of the chemistry regime (Pinder et al., 2008); hence, the traditional observable indicators provide policy-makers limited information for reducing O_3 and $PM_{2.5}$ pollution.

The sensitivity of O_3 and $PM_{2.5}$ to precursor emissions can be explored by running multiple brute-force CTM simulations. For instance, the response surface model (RSM) developed from brute-force simulations can generate a wide range of O_3 and $PM_{2.5}$ responses to precursor emissions ranging from fully controlled to doubled emissions (i.e., -100 % to 100 % change relative to the baseline emission) (Xing et al., 2011; Wang et al., 2011). Based on the RSM, the chemical response indicators of Peak Ratio (PR) and Flex Ratio (FR) have been designed to identify regimes of O_3 and $PM_{2.5}$ chemistry, respectively (see Xing et al., 2018 for detailed description of PR and FR). In contrast to the observable indicators, the PR and FR are meaningful values that represent the exact transition point at which a chemistry regime

converts to another regime. With the recent development of the polynomial function-based RSM (pf-RSM), the PR and FR can be easily calculated (Xing et al., 2018). However, this method is built on at least 20 CTM simulations; in other words, the estimating the PR and FR requires considerable computing resources. As a result, RSM use remains limited despite recent improvements in RSM efficiency (Xing et al., 2017).

Over the preceding decade, China's air quality has undergone substantial changes. In particular, the enactment of the *Air Pollution Prevention and Control Action Plan* from 2013 to 2017 greatly reduced $PM_{2.5}$ exposure (Zhao et al., 2018; Ding et al., 2019a). However, during this period, significant increases in O_3 concentrations were observed in most Chinese cities (Li et al., 2018). The rate of increase in O_3 concentration (based on the 90th percentile of daily maximum of 8-hr running average) was approximately 27 %, 19 %, and 8 % in the North China Plain (NCP), Yangtze River Delta (YRD), and Pearl River Delta (PRD), respectively (Ding et al., 2019b). Greater control over anthropogenic sources must be enforced to reduce $PM_{2.5}$ and O_3 concentrations (Lu et al., 2018). Notably, accurate quantification of the nonlinear responses of O_3 and $PM_{2.5}$ to their precursor emissions is critical and a prerequisite for effective mitigation of air pollution in China.

The design of an effective O_3 and $PM_{2.5}$ control strategy requires efficient quantification of air pollutant sensitivity to precursor emissions. Indicator studies have demonstrated that the nonlinear response of O_3 and $PM_{2.5}$ to precursors can be estimated by using ambient concentrations of related chemical species. It is expected that the response indicators originally derived from RSM predictions (i.e., PR and FR) can also be calculated using a combination of ambient concentrations of certain chemical species, enabling these indicators to become "observable" indicators rather than being dependent on numerous CTM simulations. To support the needs of policy design for O_3 and $PM_{2.5}$ control, this study developed effective indicators that not only represent O_3 and $PM_{2.5}$ chemistry but also aid in determining

the most feasible emission reduction path, similar to the benefits provided by RSM-based indicators. The flow of this study is presented in Fig. 1. The new observable response indicators were developed by investigating the link between observable and RSM-based indicators in China.

The remainder of this paper is structured as follows: Section 2 presents the detailed methods for CTM modeling, RSM configuration and response indicator development. Section 3 presents the evaluation of the performance of observable indicators in predicting the chemistry regime and the development of the observable response indicators and discusses their policy implications. Section 4 summarizes the main conclusions of this study.

2. Method

2.1. Configuration of the CTM and RSM

In this study, the Community Multi-scale Air Quality (CMAQ) model (version 5.2) was used to simulate the baseline concentrations of O_3 and $PM_{2.5}$ and their responses in numerous emission control scenarios with different emission change ratios. The simulation was conducted on a domain covering China with 27 km × 27 km horizontal resolution (Fig. 2). In 2017, January, April, July, and October were simulated to represent winter, spring, summer, and fall, respectively. An annual level was estimated as the average of the levels in these four months. The concentration data was analyzed based on the monthly average for afternoon O_3 (12:00–18:00 China Standard Time when O_3 was the highest across a day), and monthly average for 24-h $PM_{2.5}$. To approximate exposure concentrations, we also estimated population-weighted O_3 and $PM_{2.5}$ at the regional or national level by averaging the gridded concentrations weighted by the population in each grid cell. The gridded population data were obtained from the 1 km × 1 km LandScan population dataset in 2016 (Oak Ridge National Laboratory, 2013).

The anthropogenic emission data were developed by Tsinghua University by using a bottom-up method (Ding et al., 2019a), with updated activity data from the 2017 China statistical yearbook as well

as the latest application rates of end-of-pipe control technologies based on the governmental bulletin and reports. The anthropogenic emissions were gridded into 27 km × 27 km horizontal resolution to match the CMAQ model (Fig. S1). The 2017 biogenic emissions over China were generated using the Model for Emissions of Gases and Aerosols from Nature (MEGAN; version 2.04). The meteorology field, driven by the Weather Research and Forecasting Model (WRF; version 3.7), followed the same configuration as that in our previous study (Ding et al., 2019a,b), and thus included the Morrison double-moment microphysics scheme, the RRTMG radiation scheme, Kain-Fritsch cumulus cloud parameterization, the Pleim-Xiu land-surface physics scheme, and the ACM2 PBL physics scheme. We used NCEP FNL (Final) Operational Global Analysis data for the initial and boundary conditions in the WRF. The comparison with observation data from the National Climatic Data Center suggested agreeable performance of the WRF model for simulating wind speed, humidity and temperature (Table S1). The CMAQ model performance in reproducing O_3 and $PM_{2.5}$ concentrations was evaluated by comparison with the ground-based observations (Fig. S2), which suggested acceptable CMAQ model performance that met the recommended benchmark (Ding et al., 2019a,b). The normalized mean biases of CMAQ in predicting $PM_{2.5}$ and O_3 are -16.4% and -12.5% compared with monitoring data obtained from the China National Environmental Monitoring Centre. The mean fractional biases for $PM_{2.5}$ and O_3 prediction are -14.2% and -11.1%, respectively (within the benchmark of ±60%). The mean fractional errors for $PM_{2.5}$ and O_3 prediction are 21.6% and 17.0% respectively (within the benchmark of 75%). The RSM was developed based on multiple CTM simulations for various emission-control scenarios according to the brute-force method. Identical to our previous RSM studies (Xing et al., 2017, 2018), the responses of O_3 and $PM_{2.5}$ to precursor emissions were analyzed using the baseline case and 40 control scenarios using the Latin Hypercube Sample method for four control variables, namely the emission ratios of NO_x, SO_2, NH_3, and VOCs. Though the responses of O_3 and $PM_{2.5}$ to local or regional emissions vary significantly as suggested in our previous study (Xing

et al., 2011), we applied the same change ratio of each pollutant emission to all regions across China in this study. This approach is consistent with the implementation of a multi-regional joint control strategy, which is reasonable for China. The same level of local and regional emission reduction has been recommended to achieve China's aggressive air quality goals (Xing et al., 2019).

The control matrix is provided in Table S2. The range of emission changes is set as 0 to 2 to be consistent with our previous studies in which the pf-RSM performance has been well examined (Xing et al., 2011; Wang et al., 2011; Xing et al., 2018; Ding et al., 2019b). The pf-RSM performance in predicting $PM_{2.5}$ and O_3 responses has been evaluated in detail using leave-one-out cross validation as well as the out-of-sample validation method, with normalized errors all within 5% for both $PM_{2.5}$ and O_3 across the domain. Relatively large biases occurred for marginal cases, where emissions are controlled by nearly 100% and predicted concentrations are very small. These cases have limited influence on the shape of nonlinear curve of the response function. However, the RSM is developed from a suite of CMAQ simulations, and so uncertainties in the chemical mechanism used in CMAQ might influence the O_3 and $PM_{2.5}$ predictions.

2.2. RSM-based indicators of O_3 and $PM_{2.5}$ chemistry

Based on the developed pf-RSM, the nonlinear responses of O_3 and $PM_{2.5}$ concentrations to precursor emissions can be represented as follows:

$$\Delta Conc = \sum_{i=1}^{n} X_i \cdot (\Delta E_{NOx})^{a_i} \cdot (\Delta E_{SO2})^{b_i} \cdot (\Delta E_{NH3})^{c_i} \cdot (\Delta E_{VOCs})^{d_i} \quad (1)$$

where $\Delta Conc$ is the change in O_3 or $PM_{2.5}$ concentration from the baseline concentration calculated from a polynomial function of four variables (ΔE_{NOx}, ΔE_{SO2}, ΔE_{NH3}, ΔE_{VOCs}); ΔE_{NOx}, ΔE_{SO2}, ΔE_{NH3}, and ΔE_{VOCs} are the change ratios of NO_x, SO_2, NH_3, and VOC emissions (i.e., *ΔEmissions* / *Baseline_Emissions*), respectively, relative to the baseline emissions (baseline = 0); and a_i, b_i, c_i, and d_i are the nonnegative integer powers of ΔE_{NOx}, ΔE_{SO2}, ΔE_{NH3}, and ΔE_{VOCs}, respectively. X_i is the coefficient of term *i* for the 14

(n) terms listed in Table 1.

The terms used to represent $PM_{2.5}$ and O_3 responses were determined in designing the pf-RSM (Table 1). The high-degree terms of NO_x, VOCs and NH_3 represent their strong nonlinear contributions to O_3 or $PM_{2.5}$. The interaction terms of NO_x and VOC for $PM_{2.5}$ and O_3 represent the nonlinearity in atmospheric oxidations, whereas those of NO_x and NH_3 for $PM_{2.5}$ represent aerosol thermodynamics (Xing et al., 2018).

X_i was fitted by 40 CTM control scenarios for each spatial grid cell. The X_i values in the pf-RSM for annual-averaged population-weighted O_3 and $PM_{2.5}$ concentrations in 31 provinces in China are provided in Table S3 and Table S4, respectively. The terms with first degree for NOx, SO_2, NH_3, and VOCs represent the first derivative of $PM_{2.5}$ and O_3 response to each precursor emission. O_3 was more sensitive to NO_x (term X_5) and VOCs (term X_6) than to SO_2 (term X_{13}) or NH_3 (term X_{14}), and O_3 sensitivity was negative to NO_x but positive to VOCs in most provinces. $PM_{2.5}$ sensitivities to the four precursors (terms X_1, X_2, X_5 and X_{11} for VOCs, NH_3, SO_2, and NO_x, respectively) were comparable, whereas $PM_{2.5}$ sensitivity to NO_x could be negative or positive.

The nonlinearities of O_3 and $PM_{2.5}$ to precursors were mainly determined by high-order and interaction terms. To illustrate such nonlinearities further, we used a series of isopleths, as shown in Fig. 3, as an example to present the national-averaged $PM_{2.5}$ response to SO_2 and NH_3, NO_x and NH_3, as well as $PM_{2.5}$ and O_3 responses to NO_x and VOCs in different months. Strong nonlinearity was noted in $PM_{2.5}$ sensitivity to NH_3, and in O_3 and $PM_{2.5}$ sensitivities to NO_x. $PM_{2.5}$ sensitivity to NH_3 increased alongside the transition of $PM_{2.5}$ chemistry from the NH_3-rich condition (typically at high NH_3 emission ratios) to the NH_3-poor condition (typically at low NH_3 emission ratios). O_3 and $PM_{2.5}$ sensitivities to NO_x were negative under the NO_x-saturated regime (typically at high NO_x emission ratios) but became positive under the NO_x-limited regime (typically at low NO_x emission ratios). In addition, the transition points

(corresponding to the NO_x or NH_3 ratios at which the chemical regime for O_3 or $PM_{2.5}$ chemistry changed) varied by time (Fig. 3) and space (see the isopleths at different provinces in Figs S3-S6). In general, the NH_3-poor condition appears in winter because of low NH_3 evaporation and little agriculture activity which is a dominant NH_3 source. The strong NO_x-saturated condition appears in winter when photolysis is less active than in other seasons, and concentrates in industrial regions with abundant NO_x emissions.

To further quantify the aforementioned nonlinearity, two RSM-based response indicators (i.e., the PR for O_3 and FR for $PM_{2.5}$) were calculated as described in our previous studies (Xing et al., 2011, 2018; Wang et al., 2011).

For O_3, the PR can be directly calculated as follows:

$$PR = 1 + \Delta E_{NOx}|_{\frac{\partial \Delta Conc_{O3}}{\partial \Delta E_{NOx}}=0} \quad E_{NOx} \epsilon [a, b] \qquad (2)$$

where $\frac{\partial \Delta Conc_{O3}}{\partial \Delta E_{NOx}}$ is the first derivative of the $\Delta Conc_{O3}$ to ΔE_{NOx}, which can be derived as follows:

$$5 * \mathrm{X}_1 * \Delta E_{NOx}{}^4 + 4 * \mathrm{X}_2 * \Delta E_{NOx}{}^3 + 3 * \mathrm{X}_3 * \Delta E_{NOx}{}^2 + 2 * \mathrm{X}_4 * \Delta E_{NOx} + \mathrm{X}_5 = 0 \quad (3)$$

The PR is the NO_x emissions (represented as $1 + \Delta E_{NOx}$) that produce maximum O_3 concentration under the baseline VOC emissions. For PR < 1, the baseline condition is NO_x saturated, and the level of simultaneous control of VOCs to prevent an increase in O_3 levels from the NO_x controls must be understood. This level is defined by the ratio of VOCs to NO_x (i.e., VNr) corresponding to the PR and is calculated as follows:

$$VNr = r|_{\frac{\partial \Delta Conc_{O3}}{\partial \Delta E_{NOx}}=0} \quad when\ PR < 1 \quad , r = {}^{\Delta E_{VOC}}/_{\Delta E_{NOx}} \qquad (4)$$

where $\frac{\partial \Delta Conc_{O3}}{\partial \Delta E_{NOx}}$ is the first derivative of the $\Delta Conc_{O3}$ to ΔE_{NOx} . When $\Delta E_{VOC} = r \times \Delta E_{NOx}$, and ΔE_{SO2} and ΔE_{NH3} are 0, $\frac{\partial \Delta Conc_{O3}}{\partial \Delta E_{NOx}}$ can be written as follows:

$$5 * \mathrm{X}_1 * \Delta E_{NOx}{}^4 + 4 * \mathrm{X}_2 * \Delta E_{NOx}{}^3 + 3 * \mathrm{X}_3 * \Delta E_{NOx}{}^2 + 2 * \mathrm{X}_4 * \Delta E_{NOx} + \mathrm{X}_5 + \mathrm{X}_6 * \mathrm{r} + 2 * \mathrm{X}_7 *$$

$$r^2 * \Delta E_{NOx} + 3 * X_8 * r^3 * {\Delta E_{NOx}}^2 + 2 * X_9 * r * {\Delta E_{NOx}}^2 + 4 * X_{10} * r^3 * {\Delta E_{NOx}}^3 + 6 * X_{11} * r * {\Delta E_{NOx}}^5 + 3 * X_{12} * r * {\Delta E_{NOx}}^2 = 0 \quad (5)$$

Since the ΔE_{NOx} is close to 0 when the controls are taken from the baseline, we ignore the terms of ΔE_{NOx} in the first derivative function above, then it can be written as follows,

$$X_5 + X_6 * r = 0 \quad (6)$$

The VNr therefore can be calculated using the following equation:

$$VNr = -\frac{X_5}{X_6} \quad (7)$$

For $PM_{2.5}$, the FR can be directly calculated from the polynomial function of $PM_{2.5}$ by estimating the second derivative of the $PM_{2.5}$ response to NH_3 emissions without considering interaction with other pollutants (Xing et al., 2018). In this study, we selected a simplified method to calculate the FR, estimated as the corresponding NH_3 emission ratio when the $PM_{2.5}$ sensitivity to NH_3 and NO_x emissions is equal under the baseline conditions (similar to the definition in Wang et al (2011), but here we calculated the sensitivity of $PM_{2.5}$ instead of nitrate in this study):

$$FR = 1 + \Delta E_{NH3}|_{\frac{\partial \Delta Conc_{PM}}{\partial \Delta E_{NH3}} = \frac{\partial \Delta Conc_{PM}}{\partial \Delta E_{NOx}}} \quad \Delta E_{NH3} \epsilon [a, b], \Delta E_{NOx} = 0, \quad (8)$$

where $\frac{\partial \Delta Conc_{PM}}{\partial \Delta E_{NH3}}$ and $\frac{\partial \Delta Conc_{PM}}{\partial \Delta E_{NOx}}$ are the first derivatives of the $\Delta Conc_{PM}$ to ΔE_{NH3} and ΔE_{NOx}, respectively, and ΔE_{NH3} can be obtained as follows:

$$3 * X_4 * {\Delta E_{NH3}}^2 + (2 * X_3 - X_{10}) * \Delta E_{NH3} + X_2 - X_{11} = 0 \quad (9)$$

The FR is the NH_3 emissions (represented as $1 + \Delta E_{NH3}$) that correspond to the inflection point between NH_3-rich and -poor conditions under baseline NOx emissions. A FR greater than 1 indicates that the baseline condition is NH_3 poor, and a FR less than 1 indicates that the baseline condition is NH_3 rich. The extra benefit in $PM_{2.5}$ reduction (denoted as ΔC_NH_3) from simultaneous NH_3 controls in the same percentage as the required NO_x controls can be quantified as follows:

$$\Delta C\_NH_3 = \left(\frac{\partial \Delta Conc_{PM2.5}}{\partial \Delta E_{NOx}}|_{\Delta E_{NH3}=\Delta E_{NOx}}\right) - \left(\frac{\partial \Delta Conc_{PM2.5}}{\partial \Delta E_{NOx}}|_{\Delta E_{NH3}=0}\right) \quad (10)$$

where

$\frac{\partial \Delta Conc_{PM2.5}}{\partial \Delta E_{NOx}}|_{\Delta E_{NH3}=\Delta E_{NOx}}$ is the first derivative of the $\Delta Conc_{PM2.5}$ response to ΔE_{NOx} when $\Delta E_{NH3} = \Delta E_{NOx}$, and

$\frac{\partial \Delta Conc_{PM2.5}}{\partial E_{NOx}}|_{E_{NH3}=0}$ is the first derivative of the $\Delta Conc_{PM2.5}$ response to ΔE_{NOx} when $\Delta E_{NH3} = 0$.

ΔC_NH_3 (the unit is μg m^{-3} $PM_{2.5}$ per 10 % NH_3 reduction) can be calculated as follows:

$$\Delta C_{NH_3} = X_2 \times 0.1 \quad (11)$$

2.3. Observable indicators of O_3 and $PM_{2.5}$ chemistry

Zhang et al. (2009) summarized the various observable indicators with their corresponding transition values to identify O_3 and $PM_{2.5}$ chemistry: O_3 indicators were H_2O_2/HNO_3, $H_2O_2/(O_3+NO_2)$, NO_y, O_3/NO_x, O_3/NO_y, O_3/NO_z, $HCHO/NO_y$, and $HCHO/NO_2$, and the $PM_{2.5}$ indicators were the DSN, GR, and AdjGR (defined in Text S1); these indicators have been used extensively in previous research (Liu et al., 2010; Wang et al., 2011; Ye et al., 2016). In the current study, we evaluated all the aforementioned indicators except DSN (DSN is included in the definition of the AdjGR, thus it was not considered as a separate indicator in this study). The orignal transition values, summarized by Zhang et al (2009), are listed in Table 2. In the present study, we examined these transition values and compared their performance in predicting O_3 and $PM_{2.5}$ chemistry. Because the RSM-based indicators, PR and FR, are calculated using the multiple CTM simulations that use state-of-the-science representations of O_3 and $PM_{2.5}$ chemistry, these indicators were assumed to represent the true condition for comparison with the condition predicted using observable indicators. The performance of each observable indicator is described by its success rate, which is the ratio of the number of correct predictions to the total number of predictions. A correct prediction is indicated by the observable indicator providing consistent results for O_3 or $PM_{2.5}$ chemistry

as suggsted by PR or FR. The comparison is only conducted for spatial grid cells with valid PR or FR values within the range of 0 (fully controlled emissions) to 2 (double emissions).

As RSM-based indicators, the PR and FR have meaningful values that can be used to illustrate the extent of the chemistry regime. The linkage of observable indicators with the PR and FR was investigated by performing a linear-log regression of the value of the original observable indicator and the values of the PR or FR as follows:

$$log(Y) = A \cdot X + B \qquad (12)$$

where Y is an observable indicator for O_3 or $PM_{2.5}$, X is the RSM-based indicator (i.e., PR for O_3 or FR for $PM_{2.5}$), and the coefficients A and B are estimated based on statistical regression. Therefore, the observable response indicators (X') can be calculated as follows:

$$X' = \frac{log(Y)-B}{A} \qquad (13)$$

The observable response indicators have the same policy implication as that of PR or FR, but they can be directly calculated from the baseline concentrations of certain chemical species rather than being derived from multiple CTM simulations. Therefore, these indicators are considerably more efficient than are traditional RSM-based indicators.

3. Results

3.1. Evaluating observable indicator performance in predicting chemistry regimes

3.1.1. O_3

Observable indicators and the PR are compared in Fig. 4, and the performance of observable indicators in predicting O_3 chemistry is summarized in Table 2. In general, strong correlation was noted between the observable indicators and PR. The indicator with the highest annual success rate was H_2O_2/HNO_3 approximately 73.4 %, with a value of 0.2 for the transition from NO_x-saturated to NO_x-

limited conditions. However, the original transition value of 0.2 for H_2O_2/HNO_3 tended to be too low, particularly in April, July, and October (see Fig. 4a). This study found that the annual success rate of H_2O_2/HNO_3 could be increased to 80.5 % if 0.3 was used as the transition value. This finding was consistent with corresponding findings in previous studies, which have suggested the transition values of H_2O_2/HNO_3 within the range of 0.2-3.6 at different locations and in different seasons (Sillman, 1995; Sillman et al, 1997; Lu and Chang, 1998; Tonnesen and Dennis, 2000; Hammer et al, 2002; Liang et al, 2006; Zhang et al., 2009). $H_2O_2/(O_3+NO_2)$, with a transition value of 0.02, also exhibited a high annual success rate of 66.4 %; this rate could be increased to 71.1 % by applying a transition value of 0.005 because the original transition value was too high, particularly in January, April, and October (see Fig. 4b). $HCHO/NO_y$ and $HCHO/NO_2$ exhibited relatively low performance, particularly in April and July, because the original transition values appeared to be too high (Fig. 4g and h). However, the performance of $HCHO/NO_y$ and $HCHO/NO_2$ could be greatly improved by using lower transition values, with increased annual success rates as high as 76 %. The change of the transition values implies that such indicators cannot fully consider all factors that determine the O_3 chemistry by using concentrations of just two species. The transition values of the indicators NO_y, O_3/NO_x, O_3/NO_y, and O_3/NO_z were suitable for estimating annual levels if only one unique transition value was applied for all months (apparently, these transition values for O_3/NO_x, O_3/NO_y and O_3/NO_z in January, and NO_x in April and July may have been too low). However, their success rates (all < 70 %) were not as high as those of other indicators. The inferior performance of the three O_3-involved indicators (O_3/NO_x, O_3/NO_y and O_3/NO_z) may have been associated with the considerable effects of background O_3, which cannot be removed easily.

Because $H_2O_2/(O_3+NO_2)$ and $HCHO/NO_2$ exhibited good performance in predicting O_3 chemistry, this study proposed a new indicator combining these two indicators, namely $H_2O_2 \times HCHO/NO_2$, with a transition value of 0.3. The results suggested that this new indicator has the highest annual success rate,

namely 87.3 %, among all the indicators. Studies (Sillman, 1995; Tonnesen and Dennis, 2000) have suggested that HCHO is approximately proportional to the VOC reactivity (i.e., the weighted sum of the reactions of VOCs with OH) and that HCHO/NO_2 closely approximates the competition between OH reactions with VOC and NO_2 that is central to O_3 chemistry. H_2O_2 derives from a key radical termination pathway under low NO_x conditions ($HO_2 + HO_2 \rightarrow H_2O_2 + O_2$). Comparison of H_2O_2 with NO_y or HNO_3, which derives from a key radical termination pathway under high NO_x conditions, $OH + NO_2 \rightarrow HNO_3$) represents the relative abundance of VOCs to NO_x. The new hybrid indicator incorporates information from the two individual indicators and could potentially be more robust.

3.1.2 $PM_{2.5}$

We selected the GR and AdjGR as observable indicators for $PM_{2.5}$ chemistry to identify NH_3-poor or NH_3-rich conditions. Comparison of GR and AdjGR with the FR is detailed in Fig. 5. AdjGR performance was much higher than that of the GR, with a larger annual success rate of 74.1 % compared with the GR's 55.6 % (see Table 3). The transition value of the GR appeared to be too low in all months (Fig. 5a). This result was consistent with those of previous studies; the AdjGR tends to be a more robust indicator because in contrast to the GR, it does not require an assumption of full sulfate neutralization (Zhang et al., 2009). The improvement of AdjGR compared to GR is the greatest in January and the smallest in July (Table 3). This is consistent with Pinder et al. (2008) who showed that accounting for DSN is important under cold temperatures but GR and AdjGR converge for higher temperatures.

This study designed a new indicator, total ammonia ratio (TAR), where the sulfate concentration is involved in the calculation, as follows:

$$TAR = \frac{[TA]^2}{[TN]\times[TS]} = \frac{[NH_3]\times[NH_4^+]}{([HNO_3]+[NO_3^-])\times[SO_4^{2-}]}, \qquad (14)$$

where $[TN]$ and $[TS]$ are the total molar concentrations of nitrate ($[HNO_3] + [NO_3^-]$) and sulfate

336 ($[SO_4^{2-}]$), respectively, and TAR is the relative abundance of total ammonia to nitrate and sulfate, regarded
337 as the product of $[TA]/[TN]$ and $[TA]/[TS]$. To simplify the calculation, $[TA]^2$ is assumed to be the
338 product of the molar concentration of ammonia gas $[NH_3]$ and ammonium $[NH_4^+]$.

339 The performance of TAR in predicting $PM_{2.5}$ chemistry was slightly higher than that of AdjGR, as
340 demonstrated by the higher success rate of TAR than that of AdjGR in all months. The annual success rate
341 of TAR was 79.6 %, with a transition value of 10 (Table 3).

342 **3.2 Developing the observable responsive indicators**

343 **3.2.1 O_3**

344 Fig. 6 presents the log-linear regressions of the O_3 observable indicators on the PR indicator derived
345 from the RSM. In general, all observable indicators exhibited strong correlations with the PR (all except
346 NO_y presented positive correlations with the PR), with varying R^2 values (0.08 – 0.75). The indicators
347 including NO_y, O_3/NO_x, O_3/NO_y, and O_3/NO_z, which had relatively low success rates, exhibited weaker
348 correlation with the PR ($R^2 < 0.31$; Fig. 6c-f). The newly developed $H_2O_2 \times HCHO/NO_2$ indicator exhibited
349 the strongest correlation with the PR ($R^2 = 0.75$), implying that the log-linear combination of the H_2O_2,
350 HCHO, and NO_2 baseline concentrations could approximate the responsive PR indicator to quantify O_3
351 chemistry. Other indicators can also be used to approximately estimate the PR based on the regression
352 coefficients shown in Fig. 6; however, their correlations with the PR were not as strong as those with
353 $H_2O_2 \times HCHO/NO_2$.

354 To evaluate the ability of the observable PR (oPR; estimated based on $H_2O_2 \times HCHO/NO_2$) to
355 represent the spatial and temporal variation of O_3 chemistry, the spatial distribution of the PR and oPR in
356 the four study months was compared across the simulated domain (Fig. 7). The oPR successfully captured
357 the strong NO_x-saturated regime in January (PR < 1) and the NO_x-limited (PR > 1) regime in July.

In addition, the PR and oPR suggested a consistently strong NO_x-saturated regime in northern and eastern China and key regions such as the YRD and PRD. The domain-averaged oPRs were 0.97, 1.52, 1.73, and 1.37 in January, April, July, and October, respectively; these values are similar to the PRs (0.77, 1.24, 1.38, and 1.17, respectively). Thus, the oPR may approximate the PR to quantify the O_3 chemistry, even on a large spatial and temporal scale.

3.2.2. $PM_{2.5}$

The correlations between $PM_{2.5}$ observable indicators and the responsive FR indicator derived from the RSM were investigated (Fig. 8). The AdjGR has the lowest R^2 (0.40) because of its high variations for the NH_3-poor condition (Fig. 5b). A stronger positive correlation was noted between the GR and FR (R^2 = 0.57); however, the success rate of the GR was the lowest among all the indicators (the success rate of the GR increased when the transition value was set as the median value of the GR, namely 5, at an FR of 1). The TAR exhibited the strongest positive correlation with the FR (R^2 = 0.60), implying that the FR can be approximately estimated by the log-linear combination of baseline concentrations of ammonia gas, nitric acid gas, particulate ammonium, sulfate, and nitrate.

The capability of the observable FR (oFR; estimated based on the TAR indicator) in representing the spatial and temporal variation of $PM_{2.5}$ chemistry is illustrated in Fig. 9. Both the FR and oFR suggested strong NH_3-poor condition (FR > 1) in January and NH_3-rich condition (FR < 1) in April and July. The oFR suggested strong NH_3-rich condition in northern and eastern China and the Sichuan Basin; these findings were consistent with those for the FR. The domain-averaged oFRs were 1.56, 1.05, 0.86, and 1.24 in January, April, July, and October, respectively, with the strongest NH_3-poor condition in January and NH_3-rich condition in July. These findings were comparable with the FRs of 1.47, 1.16, 0.95, and 1.19 for the four study months, respectively, suggesting that the oFR can approximate the FR to quantify the $PM_{2.5}$ chemistry and its spatial and temporal variations.

3.3. Policy implications

3.3.1. O_3

The responsive PR indicator may help policy-makers to understand the status and extent of O_3 chemistry in the current scenarios. A lower PR (< 1) suggested a NO_x-saturated regime. Moreover, the VNr could be used to inform policy-makers about the level of simultaneous control of VOCs required to prevent an increase in O_3 levels from NO_x controls. In general, the VNr is negatively correlated with the PR because a lower PR implies a stronger NO_x-saturated regime, which in turn requires more simultaneous VOC control with NO_x. By contrast, a higher PR implies a weaker NO_x-saturated or even NO_x-limited regime, which requires less or no simultaneous control of VOCs with NO_x. The negative correlation between VNr and the PR was quantified by the simple linear regression of VNr on PR (Fig. S7). A high R^2 (approximately 0.82) suggested that the VNr originally derived from the RSM can also be approximately estimated from the PR or oPR.

Figure 10 presents a comparison of the VNr derived from the RSM, with the VNr calculated based on the oPR, estimated by the $H_2O_2 \times HCHO/NO_2$ indicator and denoted as oVNr. Consistent spatial and temporal variations were found for VNr and oVNr. Additional simultaneous VOC control is required in January and in northern and eastern China, and is highly correlated with the low PR (Fig. 7). The domain-averaged oVNr values were estimated to be 0.95, 0.43, 0.38, and 0.47 in January, April, July, and October, respectively, with the highest and lowest oVNr values noted in January and July, respectively. That is comparable with VNr in the four study months (i.e., 0.82, 0.46, 0.34, and 0.57, respectively).

The annual-averaged VNr and PR were also calculated for each province in China (Fig. 11). VNr was negatively correlated with the PR at the provincial level. The northern provinces, namely Heilongjiang, Xinjiang, and Liaoning required the highest VNr (1-1.2) because their PRs were very low (0.3-0.4). In the NCP, including the province of Tianjin, Hebei, Henan, Shandong, Shanxi, Inner Mongolia, and Beijing,

high VNr (0.7-0.9) was required to overcome the stronger NO_x-saturated regime (PR = 0.4-0.6). The coastal provinces, namely Fujian, and Guangdong, and middle-eastern provinces, namely Jiangxi and Hunan, also demonstrated relatively high PRs (>0.7) and low VNr (<0.3).

3.3.2. $PM_{2.5}$

Using the responsive FR indicator or its observable oFR indicator can rapidly identify NH_3-rich or NH_3-poor conditions, and this information can aid policy-makers in estimating the additional $PM_{2.5}$ benefit associated with simultaneous control of NH_3 and NO_x emissions (ΔC_NH_3). As discussed in Section 2.2, ΔC_NH_3 can be calculated from the RSM using the first derivative of the $PM_{2.5}$ responsive function to NH_3. Therefore, ΔC_NH_3 must be strongly associated with the secondary inorganic aerosol (SNA) concentration, as suggested in Fig. S8, which demonstrates a strong correlation between SNA concentration and ΔC_NH_3. The linear regression with high R^2 (>0.71) implies that the ΔC_NH_3 can be approximately calculated based on the SNA concentration.

The ΔC_NH_3 estimated based on the SNA concentration ($o\Delta C\_NH_3$; based on the regression function in Fig. S8) was compared with that derived from the RSM (Fig. 12). The $o\Delta C\_NH_3$ typically captured the spatial and temporal variation of ΔC_NH_3, suggesting large benefits in January and October, particularly in eastern China and the Sichuan Basin. The domain-averaged ΔC_NH_3 values were approximately 0.31, 0.22, 0.16, and 0.38 μg m^{-3} $PM_{2.5}$ per 10 % NH_3 reduction in January, April, July, and October respectively. In April and July, $o\Delta C\_NH_3$ presented consistent results approximately 0.21 and 0.16 μg m^{-3} $PM_{2.5}$, respectively, per 10 % NH_3 reduction, but slightly underestimated the benefits in January and October (0.24 and 0.22 μg m^{-3} $PM_{2.5}$, respectively, per 10 % NH_3 reduction).

At the annual level, ΔC_NH_3 was compared with the population-weighted $PM_{2.5}$ concentration in each province (Fig. 13). ΔC_NH_3 ranged from 0.2 to 1.2 μg m^{-3} $PM_{2.5}$ per 10 % NH_3 reduction. In addition, the provinces with higher $PM_{2.5}$ exposure exhibited additional benefits from NH_3 reductions (i.e., high

427 ΔC_NH_3), particularly in Hunan, Shandong, Tianjin, Jiangxi, Anhui, Henan, and Hubei where ΔC_NH_3
428 was > 0.8 μg m^{-3} $PM_{2.5}$ per 10 % NH_3 reduction. These benefits from simultaneous NH_3 control were
429 substantial enough to be considered in these regions for achieving the national ambient $PM_{2.5}$ target (35
430 μg m^{-3}).

431 **3.3.3. Cobenefits of NO_x and VOC control in reducing O_3 and $PM_{2.5}$**

432 NO_x and VOCs are major precursors for O_3 and $PM_{2.5}$, and effectively controlling their emissions
433 can lead to cobenefits in reducing O_3 and $PM_{2.5}$. The PR results suggest strong NO_x-saturated regimes in
434 northern and eastern China including key regions such as the Sichuan Basin, YRD, and PRD, where
435 simultaneous VOC control with a certain VOC-to-NO_x ratio is required to prevent increases in O_3 levels
436 from the NO_x controls. $PM_{2.5}$ senstivity to NO_x can be negative under a strong NO_x-saturated regime; this
437 effect is not as significant as it is for O_3 (Fig. 3). We quantified the nonlinearity of $PM_{2.5}$ sensitivity to NO_x
438 by using the same PR concept but for $PM_{2.5}$ response (Text S2); Fig. S9 presents the spatial distribution
439 of the PR to identify $PM_{2.5}$ sensitivity to NO_x emission in the four study months. The PR values for $PM_{2.5}$
440 were > 1 in April, July, and October in all grid cells across China, suggesting that NO_x control is always
441 beneficial for $PM_{2.5}$ reduction during these months. Even in January, the PR for $PM_{2.5}$ (0.4-0.8 in eastern
442 and northern China) remains larger than that for O_3 (0.2-0.6 in eastern and northern China), implying that
443 the suggested VNr for O_3 was high enough to overcome the potential limitations on $PM_{2.5}$ reduction from
444 NO_x control.

445 To explore the cobenefits of reducing O_3 and $PM_{2.5}$ after simultaneous control of NO_x and VOCs,
446 we investigated the effectiveness of six control pathways with various VOC-to-NO_x ratios including 0,
447 0.2, 0.4, 0.6, 0.8 and 1.0 (Fig. 14). In general, O_3 and $PM_{2.5}$ concentrations can be reduced in all months
448 through simultaneous control of NO_x and VOC emissions, although different VNr and control levels are
449 required in different months. In January (under strongly NO_x-saturated conditions), reductions in $PM_{2.5}$

and O_3 require VOC emission controls in addition to NOx controls to prevent potential disbenefits associated with the nonlinear chemistry. The smaller VNr required for $PM_{2.5}$ (~0.4) than for O_3 (~1.0) in this case might be associated with the smaller PR for $PM_{2.5}$ as well as the additional benefit of VOC controls in reducing secondary organic aerosols. Apparently, a larger VNr control ratio and greater emission control is required in January compared with other months. In Fig. 14(a), only one pathway can achieve simultaneous reduction in O_3 and $PM_{2.5}$ concentrations (i.e., the pathway with VNr equal to 1 and at the far end of the pathway, with reduction rates > 80%). In April and October, simultaneous VOC controls were still required for O_3 (VNr = 0.2-0.6) but not for $PM_{2.5}$. In July when NO_x-limited regime was dominant, the NO_x control was critical because the VOC controls had little effect on either O_3 or $PM_{2.5}$. At the annual level, the simultaneous VOC controls (40 % of the NO_x controls) led to cobenefits in reducing both O_3 and $PM_{2.5}$ at the national level. However, VNr varied significantly in different seasons, suggesting that considering the seasonality of O_3 and $PM_{2.5}$ chemistry is necessary for design of a season-specific control strategy.

4. Summary and conclusion

Compared with conducting multiple CTM simulations, the indicator method proved more efficient in identifying the chemical regime in the current scenarios. However, the traditional indicators are not as useful as the RSM-based PR and FR indicators for policy-makers to infer feasible emission reduction paths. Therefore, this study quantified the relationship between RSM-based and traditional-observable indicators and developed new observable response indicators, the oPR and oFR, which can be used to quantify the nonlinearity of O_3 and $PM_{2.5}$ response to precursor emissions. Similar to the traditional indicators, the oPR and oFR can be easily calculated using a combination of ambient concentrations of certain chemical species obtained from surface-monitored observations, modeling simulations, or even satellite retrievals. In addition, the observable responsive indicators can not only rapidly identify the

chemical regime but also provide policy-makers with useful information, such as simultaneous VOC controls to prevent increases in O_3 levels from NO_x controls under the NO_x-saturated regime (i.e., VNr), as well as the additional benefit of simultaneously reducing NH_3 alongside NO_x control in $PM_{2.5}$ reductions (i.e., ΔC_NH_3). Since the indicators are developed from simulations with spatially uniform emission controls across the country, they are especially useful for providing quick estimates of the potential benefits or risks from uniform controls. These estimates can also provide a basis to design more localized control strategies for particular regions.

This study proposed a new O_3-chemistry indicator, namely $H_2O_2 \times HCHO/NO_2$, and $PM_{2.5}$-chemistry indicator, namely the TAR, both of which exhibited the highest success rates among all the indicators. This study also suggested that the log-linear combinations of baseline H_2O_2, HCHO, and NO_2 concentrations could provide an approximate PR to quantify O_3 chemistry spatially and temporally. Similarly, the log-linear combination of baseline concentrations of ammonia gas, nitric acid gas, particulate ammonium, sulfate and nitrate can be used to approximately estimate the FR for $PM_{2.5}$ chemistry. The VNr was highly correlated with the PR, suggesting that a stronger NO_x-saturated regime requires greater VOC control accompanied by NO_x control. The positive correlation between ΔC_NH_3 and the population-weighted $PM_{2.5}$ concentration suggested that a province with high $PM_{2.5}$ exposure can gain greater benefits from NH_3 reduction. Finally, simultaneous control of NO_x and VOC could reduce both O_3 and $PM_{2.5}$ throughout the year, and an effective control pathway (VNr = 0.4) could lead to the cobenefits of reducing both O_3 and $PM_{2.5}$. However, VNr varied significantly among the seasons and provinces, suggesting the necessity of considering the seasonality of chemistry and of designing a more localized control strategy for each province. We note that the discrepency between the observable indicator and the responsive indicator might also be influcenced by uncertainties in the chemical mechanism of CMAQ as well as prediction errors of the pf-RSM. The new indicators were designed based on the existing

chemical mechanism, and the transition values might be refined in the future as our understanding of atmospheric chemical processes improves.

In conclusion, the two unique aspects of this study are as follows. First, quantification of the correlation of observable indicators with responsive indicators (Fig. 5 and 7) implied that the traditional observable indicators, based on monitored or satellite-retrieved concentrations, can be used to quantify the nonlinearity of $PM_{2.5}$ and O_3 to precursor emission and provide useful policy implications. Second, this study reported a promising method for efficiently establishing $PM_{2.5}$- and O_3- responsive functions to precursors for traditional responsive or reduced-form modeling studies. This study suggested that the PR or FR (a combination of coefficients in the polynomial functions in the pf-RSM) can be approximately estimated using the ambient concentration of certain chemical species. Similarly, all coefficients in polynomial functions can be calculated based on a set of ambient concentrations of certain chemical species. The simple log-linear regression method used in this study demonstrated the possibility that even in the presence of uncertainties in prediction, more advanced data analytics technologies such as deep learning may improve performance in future.

Data availability

The pf-RSM outputs and code package are available upon request from the corresponding author.

Author contribution

These authors contributed equally to this work: Jia Xing & Dian Ding. JX designed the methodology and wrote the paper. DD conducted the modeling experiment and analyzed the data. SW provided ideas and financial support and edited the paper. ZD and YZ helped with the modeling experiment. JK, CJ and JH provided ideas and edited the paper.

Acknowledgements

This work was supported in part by National Key R & D program of China (2017YFC0210006), National Natural Science Foundation of China (21625701&51861135102), National Research Program for Key Issues in Air Pollution Control (DQGG0301& DQGG0204), and Shanghai Environmental Protection Bureau (2016-12). This work was completed on the "Explorer 100" cluster system of Tsinghua National Laboratory for Information Science and Technology.

Disclaimer

Although this work was reviewed by EPA and approved for publication, the views in the article are those of the authors alone and do not necessarily reflect the policy of the Agency. Mention of commercial products does not constitute endorsement by the Agency.

Reference

Ansari, A. S., and S. N. Pandis: Response of inorganic PM to precursor concentrations, Environ. Sci. Technol., 32, 2706–2714, 1998.

Cohan, D.S., Hakami, A., Hu, Y., Russell, A.G.: Nonlinear response of ozone to emissions: source apportionment and sensitivity analysis. Environ. Sci. Technol., 39, 6739-6748, 2005.

Cohen, A.J., Brauer, M., Burnett, R., Anderson, H.R., Frostad, J., Estep, K., Balakrishnan, K., Brunekreef, B., Dandona, L., Dandona, R., Feigin, V.: Estimates and 25-year trends of the global burden of disease attributable to ambient air pollution: an analysis of data from the Global Burden of Diseases Study 2015. The Lancet, 389(10082), 1907-1918, 2017.

Dennis, R.L., Bhave, P.V. and Pinder, R.W. Observable indicators of the sensitivity of PM2. 5 nitrate to emission reductions—Part II: Sensitivity to errors in total ammonia and total nitrate of the CMAQ-predicted non-linear effect of SO2 emission reductions. Atmospheric Environment, 42(6), pp.1287-1300, 2008.

Ding, D., Xing, J., Wang, S., Liu, K. and Hao, J.: Estimated Contributions of Emissions Controls, Meteorological Factors, Population Growth, and Changes in Baseline Mortality to Reductions in Ambient PM 2.5 and PM 2.5-Related Mortality in China, 2013–2017. Environmental health perspectives, 127(6), 067009, 2019a.

Ding, D., Xing, J., Wang, S., Chang, X. and Hao, J.: Impacts of emissions and meteorological changes on China's ozone pollution in the warm seasons of 2013 and 2017, Front. Environ. Sci. Eng. 2019, 13(5): 76, 2019b.

Forouzanfar, M.H., Alexander, L., Anderson, H.R., Bachman, V.F., Biryukov, S., Brauer, M., Burnett, R., Casey, D., Coates, M.M., Cohen, A., Delwiche, K.: Global, regional, and national comparative risk assessment of 79 behavioural, environmental and occupational, and metabolic risks or clusters of risks in 188 countries, 1990–2013: a systematic analysis for the Global Burden of Disease Study 2013. The Lancet, 386 (10010), 2287–2323, 2015.

Freas, W. P., Martinez, E. L., Meyer, E. L., Possiel, N. C., and Sennett, D. H.: Procedures for quantifying relationships between photochemical oxidants and precursors: supporting documentation, 1978.

Friedlander, S.K. Smoke, dust and haze: Fundamentals of aerosol behavior. New York, Wiley-Interscience, 1977. 333pp.

Fuhrer, J., Val Martin, M. , Mills, G. , Heald, C.L., Harmens, H., Hayes, F., Sharps, K., Bender, J., Ashmore, M.R.: Current and future ozone risks to global terrestrial biodiversity and ecosystem processes. Ecology and evolution, 6(24), 8785-8799, 2016.

Gipson, G. L., Freas, W. P., Kelly, R. F., and Meyer, E. L.: Guideline for use of city-specific EKMA in preparing ozone SIPs. EPA-450/4-80-027, US Environmental Protection Agency, Research Triangle Park, North Carolina, USA, 1981.

Hakami, A., Odman, M.T., Russell, A.G.: Nonlinearity in atmospheric response: A direct sensitivity analysis approach. Journal of Geophysical Research: Atmospheres, 109(D15), 2004.

Hammer, M.U., Vogel, B. and Vogel, H.: Findings on H2O2/HNO3 as an indicator of ozone sensitivity in Baden-Württemberg, Berlin-Brandenburg, and the Po valley based on numerical simulations. Journal of Geophysical Research: Atmospheres, 107(D22), 2002.

Jiménez, P. and Baldasano, J.M.: Ozone response to precursor controls in very complex terrains: Use of photochemical indicators to assess O3-NOx-VOC sensitivity in the northeastern Iberian Peninsula. Journal of Geophysical Research: Atmospheres, 109(D20), 2004.

Jin, X., Fiore, A.M., Murray, L.T., Valin, L.C., Lamsal, L.N., Duncan, B., Folkert Boersma, K., De Smedt, I., Abad, G.G., Chance, K. and Tonnesen, G.S.: Evaluating a Space-Based Indicator of Surface Ozone-NOx-VOC Sensitivity Over Midlatitude Source Regions and Application to Decadal Trends. Journal of Geophysical Research: Atmospheres, 122(19), 2017.

Li, K., Jacob, D.J., Liao, H., Shen, L., Zhang, Q. and Bates, K.H.: Anthropogenic drivers of 2013–2017 trends in summer surface ozone in China. *Proceedings of the National Academy of Sciences*, *116*(2), pp.422-427, 2019.

Liang, J., Jackson, B. and Kaduwela, A.: Evaluation of the ability of indicator species ratios to determine the sensitivity of ozone to reductions in emissions of volatile organic compounds and oxides of nitrogen in northern California. Atmospheric Environment, 40(27), pp.5156-5166, 2006.

Liu, X.H., Zhang, Y., Xing, J., Zhang, Q., Wang, K., Streets, D.G., Jang, C., Wang, W.X., Hao, J.M.: Understanding of regional air pollution over China using CMAQ, part II. Process analysis and sensitivity of ozone and particulate matter to precursor emissions. Atmospheric Environment, 44(30), 3719-3727, 2010.

Lu, C.H. and Chang, J.S.: On the indicator-based approach to assess ozone sensitivities and emissions features. Journal of Geophysical Research: Atmospheres, 103(D3), pp.3453-3462, 1998.

Lu, X., Hong, J., Zhang, L., Cooper, O. R., Schultz, M. G., Xu, X., Wang, T., Gao, M., Zhao, Y., and Zhang, Y.: Severe Surface Ozone Pollution in China: A Global Perspective, Environmental Science & Technology Letters, 5, 487-494, 10.1021/acs.estlett.8b00366, 2018.

Megaritis, A.G., Fountoukis, C., Charalampidis, P.E., Pilinis, C. and Pandis, S.N.: Response of fine particulate matter concentrations to changes of emissions and temperature in Europe. Atmospheric Chemistry and Physics, 13(6), 3423-3443, 2013.

Milford, J. B., Gao, D. F., Sillman, S., Blossey, P., and Russell, A. G.: Total reactive nitraogen (NOy) as an indicator of the sensitivity of ozone to reductions in hydrocarbon and NOx emissions, Journal of Geophysical Research-Atmospheres, 99, 3533-3542, 10.1029/93jd03224, 1994.

Myhre, G., Shindell, D., Bréon, F.M., Collins, W., Fuglestvedt, J., Huang, J., Koch, D., Lamarque, J.F., Lee, D., Mendoza, B., Nakajima, T. Anthropogenic and Natural Radiative Forcing. In: Climate Change 2013: The Physical Science Basis. Contribution of Working Group I to the Fifth Assessment Report of the Intergovernmental Panel on Climate Change, T.F. Stocker et al, Eds. Cambridge Univ. Press, 2013, 659-740.

Oak Ridge National Laboratory. Landscan global population dataset 2012. Oak Ridge, Tennessee: Oak Ridge National Laboratory, 2013

Peng, Y.P., Chen, K.S., Lai, C.H., Lu, P.J. and Kao, J.H.: Concentrations of H2O2 and HNO3 and O3–VOC–NOx sensitivity in ambient air in southern Taiwan. Atmospheric Environment, 40(35), pp.6741-6751, 2006.

Pinder, R.W., Dennis, R.L. and Bhave, P.V.: Observable indicators of the sensitivity of PM2. 5 nitrate to emission reductions—Part I: Derivation of the adjusted gas ratio and applicability at regulatory-relevant time scales. Atmospheric Environment, 42(6), pp.1275-1286, 2008.

Pun, B.K., Seigneur, C., Bailey, E.M., Gautney, L.L., Douglas, S.G., Haney, J.L., Kumar, N.: Response of atmospheric particulate matter to changes in precursor emissions: a comparison of three air quality models. Environmental science & technology, 42(3), 831-837, 2007.

Seinfeld, J.H. and Pandis, S.N.: Atmospheric chemistry and physics: from air pollution to climate change. John Wiley & Sons, 2012.

Sillman, S.: The use of NO y, H2O2, and HNO3 as indicators for ozone-NO x-hydrocarbon sensitivity in urban locations. Journal of Geophysical Research: Atmospheres, 100(D7), pp.14175-14188., 1995.

Sillman, S., He, D., Cardelino, C. and Imhoff, R.E.: The use of photochemical indicators to evaluate ozone-NOx-hydrocarbon sensitivity: Case studies from Atlanta, New York, and Los Angeles. *Journal of the Air & Waste Management Association*, *47*(10), pp.1030-1040, 1997.

Sillman, S., and D. He, Some theoretical results concerning O3-NOx-VOC chemistry and NOx-VOC indicators, J. Geophys. Res., 107(D22), 4659, doi:10.1029/2001JD001123, 2002.

Sun, Y., Liu, C., Palm, M., Vigouroux, C., Notholt, J., Hu, Q., Jones, N., Wang, W., Su, W., Zhang, W., Shan, C., Tian, Y., Xu, X., De Mazière, M., Zhou, M., and Liu, J.: Ozone seasonal evolution and photochemical production regime in the polluted troposphere in eastern China derived from high-resolution Fourier transform spectrometry (FTS) observations, Atmos. Chem. Phys., 18, 14569-14583, https://doi.org/10.5194/acp-18-14569-2018, 2018.

Takahama, S., Wittig, A.E., Vayenas, D.V., Davidson, C.I. and Pandis, S.N.: Modeling the diurnal variation of nitrate during the Pittsburgh Air Quality Study. Journal of Geophysical Research: Atmospheres, 109(D16), 2004.

Tonnesen, G.S. and Dennis, R.L.: Analysis of radical propagation efficiency to assess ozone sensitivity to hydrocarbons and NO x: 2. Long-lived species as indicators of ozone concentration sensitivity. Journal of Geophysical Research: Atmospheres, 105(D7), pp.9227-9241, 2000.

Wang, J., Xing, J., Mathur, R., Pleim, J.E., Wang,, S., Hogrefe, C., Gan, C.M., Wong, D.C., Hao, J.: Historical trends in PM2.5-related premature mortality during 1990–2010 across the northern hemisphere. Environmental health perspectives, 125(3), 400pp, 2017.

Wang, S. X., Xing, J., Jang, C., Zhu, Y., Fu, J.S., Hao, J.: Impact assessment of ammonia emissions on inorganic aerosols in east China using response surface modeling technique. Environ. Sci. Technol., 45, 9293–9300, 2011.

Wang, S., Zhao, M., Xing, J., Wu, Y., Zhou, Y., Lei, Y., He, K., Fu, L., & Hao, J.: Quantifying the air pollutants emission reduction during the 2008 Olympic Games in Beijing. Environmental science & technology, 44(7), 2490-2496, 2010.

West, J.J., Ansari, A.S., Pandis, S.N. Marginal PM25: nonlinear aerosol mass response to sulfate reductions in the Eastern United States. Journal of the Air & Waste Management Association, 49(12), 1415-1424, 1999.

Xing, J., Wang, S. X., Jang, C., Zhu, Y., and Hao, J. M.: Nonlinear response of ozone to precursor emission changes in China: a modeling study using response surface methodology, Atmospheric Chemistry and Physics, 11, 5027-5044, 10.5194/acp-11-5027-2011, 2011.

Xing, J., Ding, D., Wang, S., Zhao, B., Jang, C., Wu, W., Zhang, F., Zhu, Y., and Hao, J. Quantification of the enhanced effectiveness of NOx control from simultaneous reductions of VOC and NH3 for reducing air pollution in the Beijing–Tianjin–Hebei region, China, Atmos. Chem. Phys., 18, 7799-7814, https://doi.org/10.5194/acp-18-7799-2018, 2018.

Xing, J., Wang, S., Zhao, B., Wu, W., Ding, D., Jang, C., Zhu, Y., Chang, X., Wang, J., Zhang, F. and Hao, J.: Quantifying Nonlinear Multiregional Contributions to Ozone and Fine Particles Using an Updated Response Surface Modeling Technique. Environmental science & technology, 51(20),11788-11798, 2017.

Xing, J., Zhang, F., Zhou, Y., Wang, S., Ding, D., Jang, C., Zhu, Y. and Hao, J.: Least-cost control strategy optimization for air quality attainment of Beijing–Tianjin–Hebei region in China. *Journal of environmental management*, *245*, 95-104, 2019.

Ye, L., Wang, X., Fan, S., Chen, W., Chang, M., Zhou, S., Wu, Z. and Fan, Q.: Photochemical indicators of ozone sensitivity: application in the Pearl River Delta, China. Frontiers of Environmental Science & Engineering, 10(6), p.15, 2016.

Zhang, J., Wang, T., Chameides, W. L., Cardelino, C., Kwok, J., Blake, D. R., Ding, A., and So, K. L.: Ozone production and hydrocarbon reactivity in Hong Kong, Southern China, Atmos. Chem. Phys., 7, 557-573, https://doi.org/10.5194/acp-7-557-2007, 2007.

Zhang, Y., Wen, X. Y., Wang, K., Vijayaraghavan, K., and Jacobson, M. Z.: Probing into regional O-3 and particulate matter pollution in the United States: 2. An examination of formation mechanisms through a process analysis technique and sensitivity study, Journal of Geophysical Research-Atmospheres, 114, 31, 10.1029/2009jd011900, 2009.

Zhao, B., Wang, S.X., Xing, J., Fu, K., Fu, J.S., Jang, C., Zhu, Y., Dong, X.Y., Gao, Y., Wu, W.J., Wang, J.D.: Assessing the nonlinear response of fine particles to precursor emissions: development and application of an extended response surface modeling technique v1.0. Geosci. Model Dev., 8, 115-128, 2015.

Zhao, B., Zheng, H., Wang, S., Smith, K.R., Lu, X., Aunan, K., Gu, Y., Wang, Y., Ding, D., Xing, J. and Fu, X. Change in household fuels dominates the decrease in PM2. 5 exposure and premature mortality in China in 2005–2015. Proceedings of the National Academy of Sciences, 115(49), pp.12401-12406, 2018.

681

682 **Table 1.** Terms in the pf-RSM design for O_3 and $PM_{2.5}$

Term	O_3	$PM_{2.5}$
1	NO_x^5	VOC
2	NO_x^4	NH_3
3	NO_x^3	NH_3^2
4	NO_x^2	NH_3^3
5	NO_x	SO_2
6	VOC	VOC^2
7	VOC^2	NO_xVOC
8	VOC^3	NO_x^2VOC
9	NO_xVOC	NO_x^4VOC
10	NO_xVOC^3	NO_xNH_3
11	NO_x^5VOC	NO_x
12	NO_x^2VOC	NO_x^2
13	SO_2	NO_x^3
14	NH_3	NO_x^4

683

684

685

686 **Table 2.** Summary of observable indicators and their performances in predicting O_3 chemistry

Indicator		success rate at TV (%)						success rate at TV' (%)				
	TV*	Jan	Apr	Jul	Oct	ANN	TV'	Jan	Apr	Jul	Oct	ANN
H_2O_2/HNO_3	0.2	68.8	74.9	89.0	60.8	73.4	**0.3**	77.9	83.0	90.4	70.6	80.5
$H_2O_2/(O_3+NO_2)$	0.02	81.1	41.9	85.4	57.4	66.4	**0.005**	69.2	73.3	88.8	53.3	71.1
NO_y	5	38.9	47.8	87.8	40.9	53.8	-	-	-	-	-	-
O_3/NO_x	15	56.5	75.8	58.8	71.7	65.7	-	-	-	-	-	-
O_3/NO_y	7	60.7	65.8	23.3	68.2	54.5	-	-	-	-	-	-
O_3/NO_z	7	43.5	75.0	76.4	67.0	65.5	-	-	-	-	-	-
$HCHO/NO_y$	0.28	83.9	32.5	19.4	50.9	46.7	**0.1**	66.7	77.7	86.3	75.6	76.6
$HCHO/NO_2$	1	87.3	49.7	27.4	73.8	59.6	**0.5**	75.7	77.2	69.1	82.2	76.1
$H_2O_2 \times HCHO/NO_2$	-	-	-	-	-	-	**0.3**	92.3	81.6	89.5	86.0	87.3

687 * TV- transition value as summaried in Zhang et al (2009); TV' - transition value proposed in this study

688

689

690

691 **Table 3.** Summary of observable indicators and their performances in predicting $PM_{2.5}$ chemistry

Indicator		success rate (%)				
	TV	Jan	Apr	Jul	Oct	ANN
Gas ratio (GR)	1*	51.7	59.3	69.6	41.7	55.6
Adjusted Gas ratio (AdjGR)	1*	81.8	73.3	74.0	67.5	74.1
Total Ammonia Ratio (TAR)	10**	86.2	77.5	80.6	74.0	79.6

692 * TV- transition value as proposed in Zhang et al (2009);

693 ** TV- transition value as proposed in this study

694

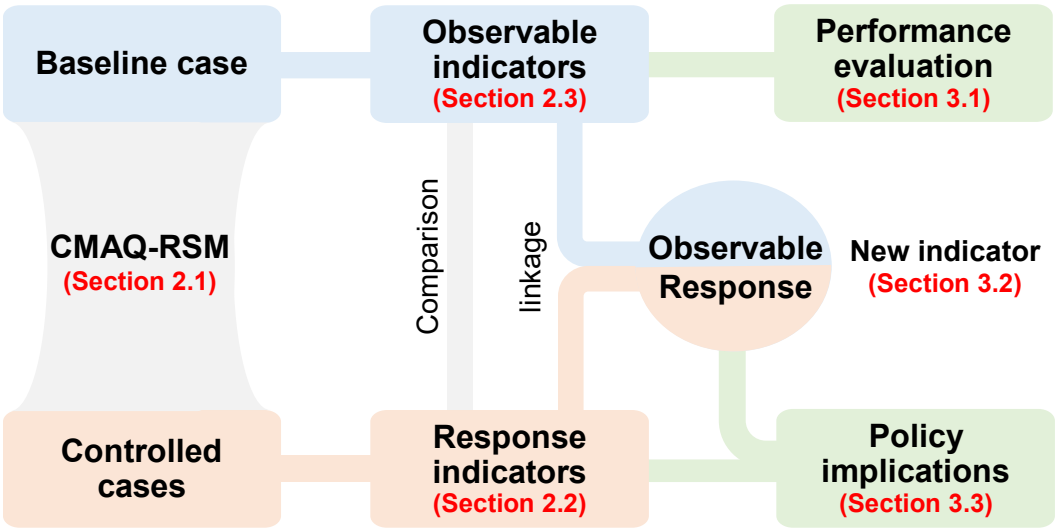

Figure 1. Flow of observable response indicator development and application

Figure 2. Simulation domain over mainland China (27 × 27-km^2 resolution, 182 × 232 grid cells). The 31 provinces are BJ-Beijing; TJ-Tianjin; HEB- Hebei; SX-Shanxi; IM-Inner Mongolia; LN- Liaoning; JL- Jilin; HLJ-Helongjiang; SH- Shanghai; JS-Jiangsu; ZJ-Zhejiang; AH- Anhui; FJ- Fujian; JX-Jiangxi; SD- Shandong; HEN- Henan; HUB-Hubei; HUN- Hunan; GD-Guangdong; GX- Guangxi; HN-Hainan; CQ- Chongqing; SC- Sichuan; GZ-Guizhou; YN- Yunnan; TB- Tibet; SHX-Shaanxi; GS-Gansu; QH-Qinghai; NX- Ningxia; and XJ-Xinjiang)

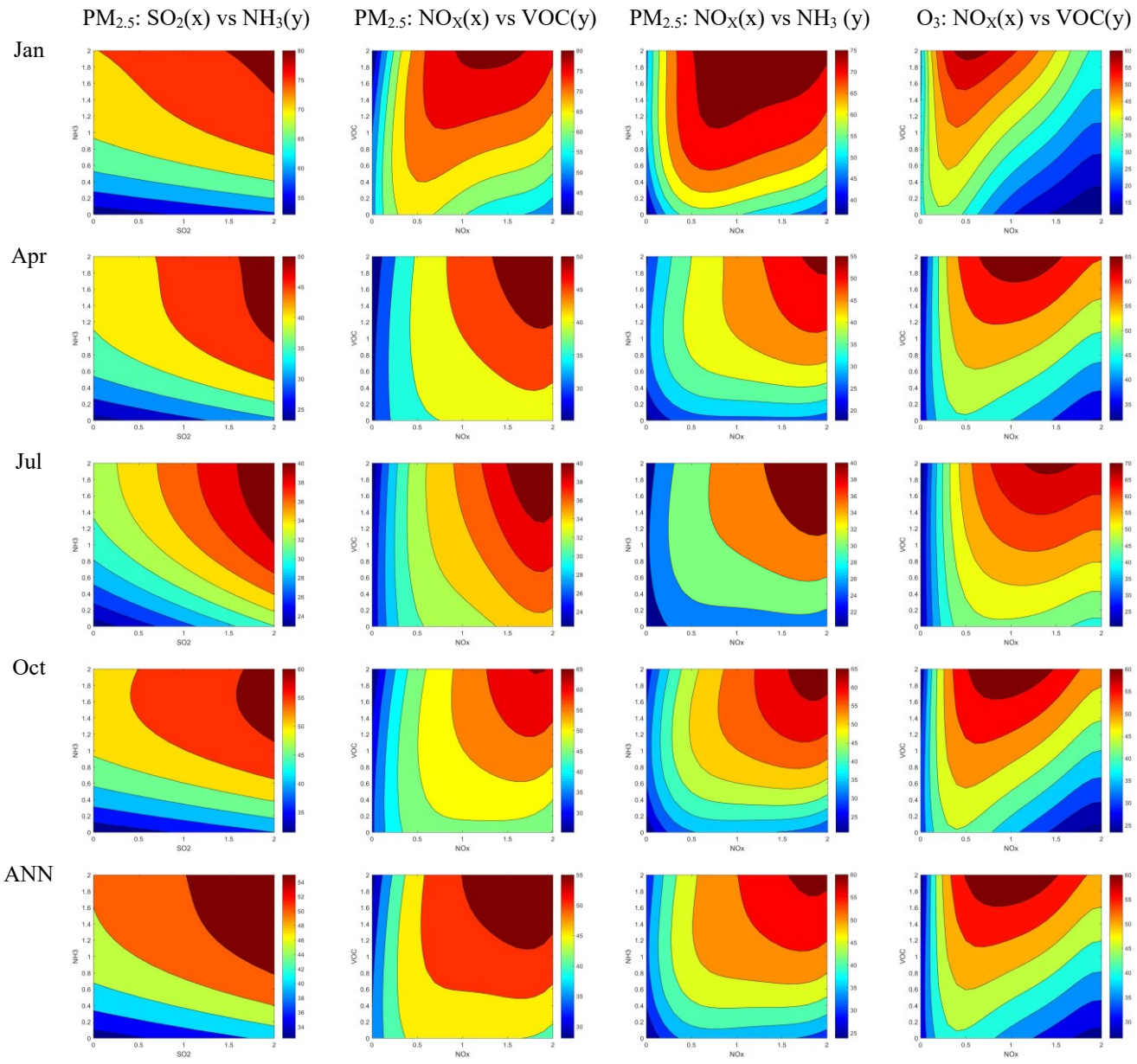

Figure 3. Isopleth of population-weighted $PM_{2.5}$ and daytime O_3 to precursor emission change in different months. (The x- and y- axes represent precursor emission rates with a baseline of 1, applied to all grid cells in China; background colors represent the population-weighted $PM_{2.5}$ and daytime O_3 concentrations in China, with units of μg m^{-3} for $PM_{2.5}$ and ppb for O_3)

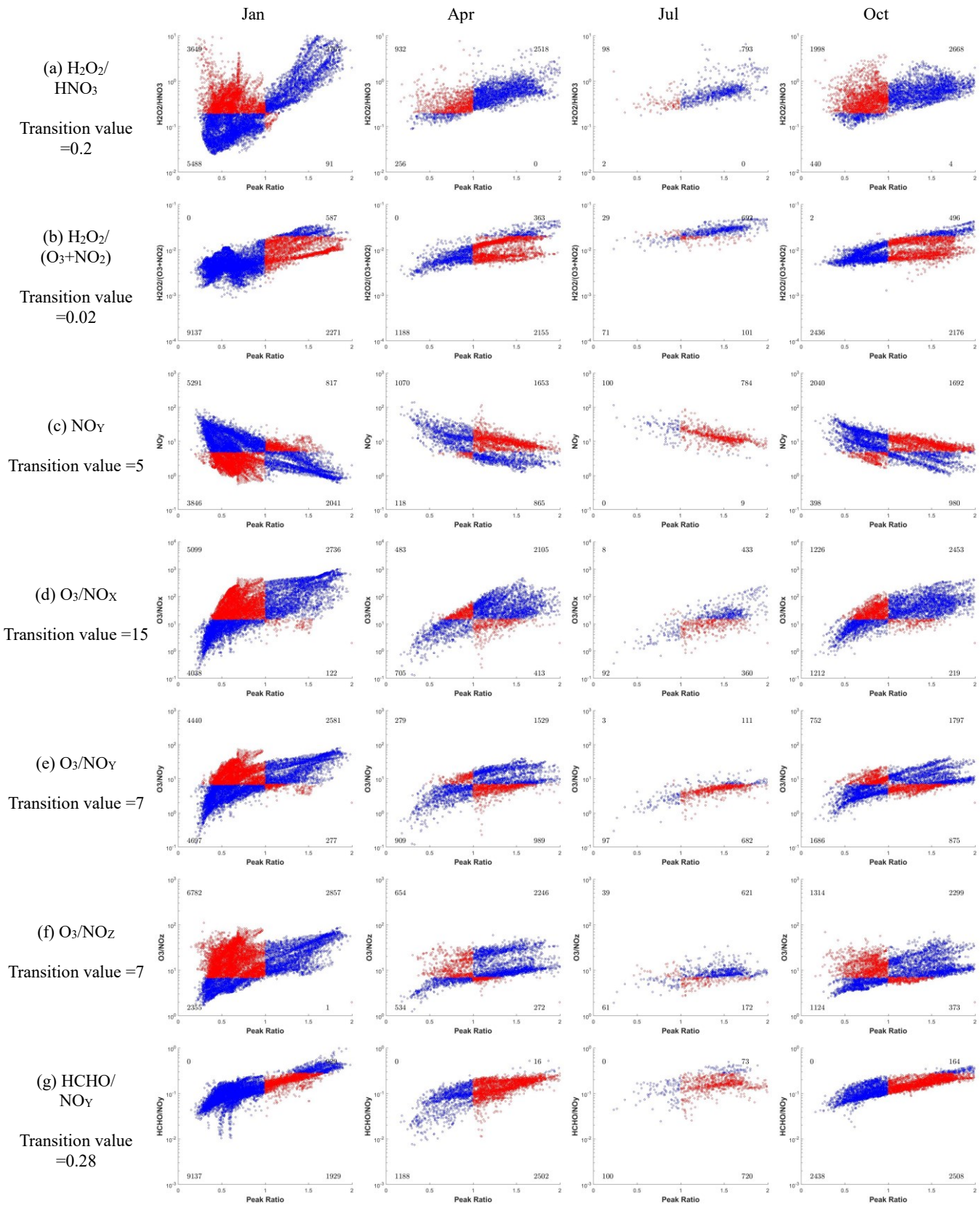
Jan
Apr
Jul
Oct
(a) H2O2/ HNO3
Transition value =0.2
(b) H2O2/ (O3+NO2)
Transition value =0.02
(c) NOY
Transition value =5
(d) O3/NOX
Transition value =15
(e) O3/NOY
Transition value =7
(f) O3/NOZ
Transition value =7
(g) HCHO/ NOY
Transition value =0.28
Peak Ratio

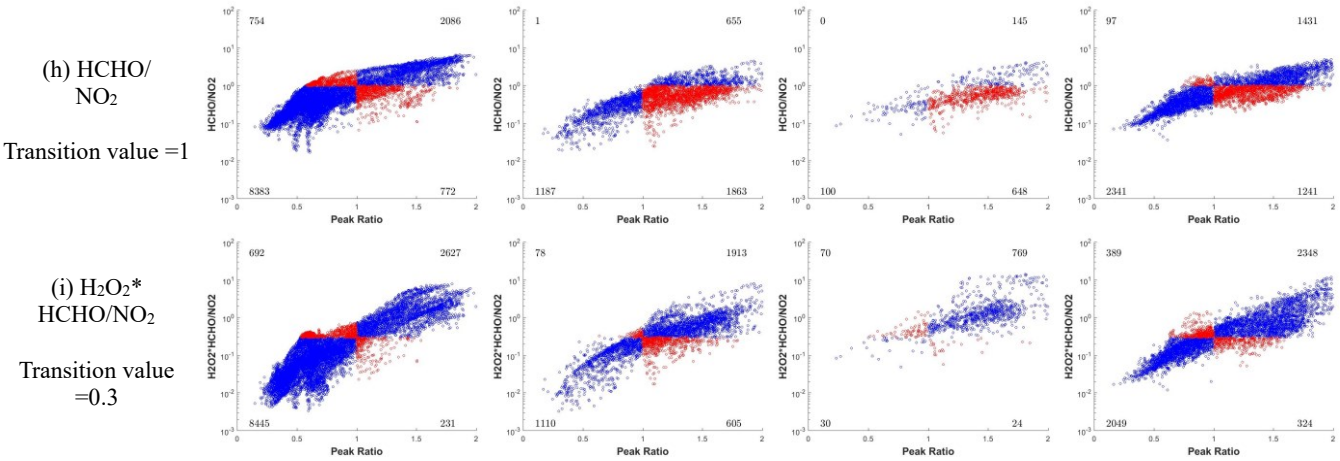

Figure 4. Performance of observable indicators in predicting O_3 chemistry. The x-axis represents the PR values where the transition value is 1, and the y-axis represents the observable indicators. The blue dots represent the grids where O_3 chemistry is successfully predicted by the observable indicator; the red dots represent the grids where the observable indicator fails to predict O_3 chemistry. The numbers in the four corners represent the grid number in each section; the number in July is much lower than those in the other months because most grids are located at the NO_x-limited regime with PR > 2 in July.

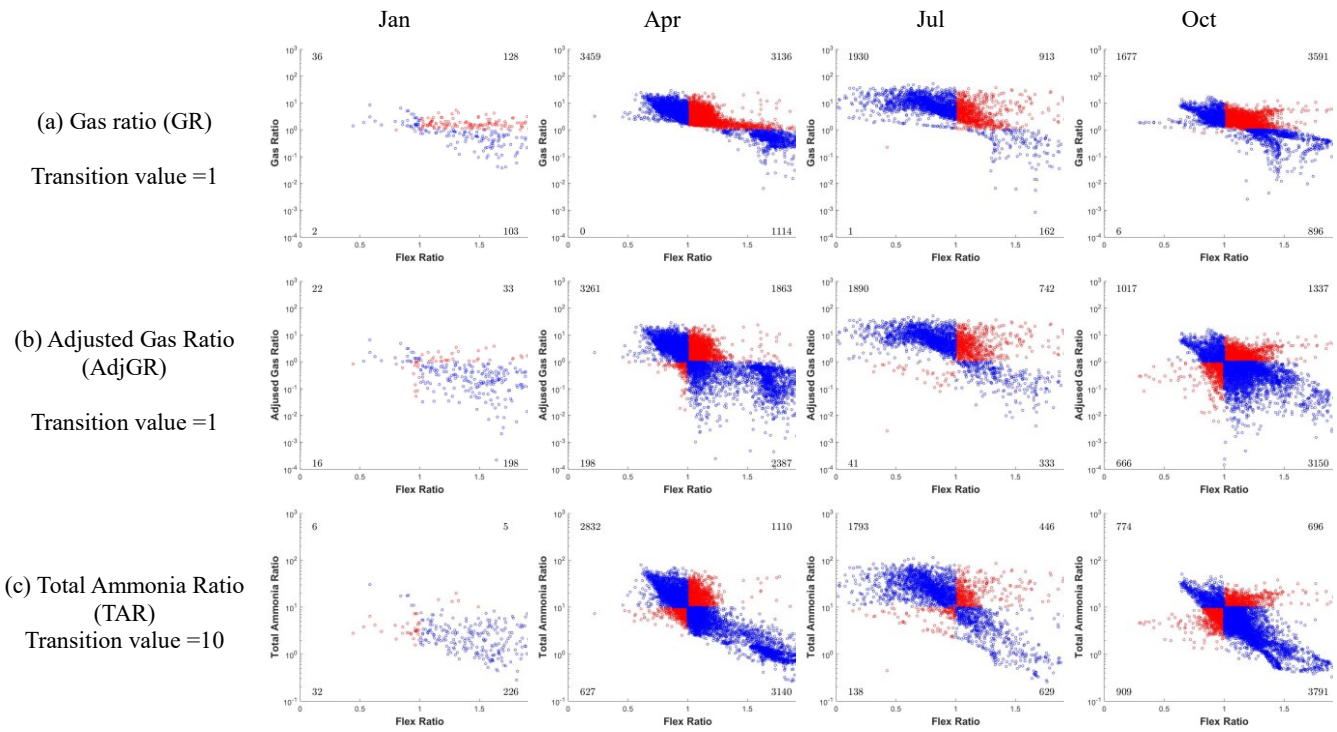

718 **Figure 5.** Performance of observable indicators in predicting $PM_{2.5}$ chemistry. The x-axis represents the
719 FR values where the transition value is 1, and the y-axis represents the observable indicators. The blue
720 dots represent the grids where $PM_{2.5}$ chemistry is successfully predicted by the observable indicator; the
721 red dots represent the grids where the observable indicator fails to predict $PM_{2.5}$ chemistry. The numbers
722 in the four corners represent the grid number in each section; the number in January is much lower than
723 those in the other months because most grids are located at the NH_3-poor condition with FR>2 in
724 January.

725

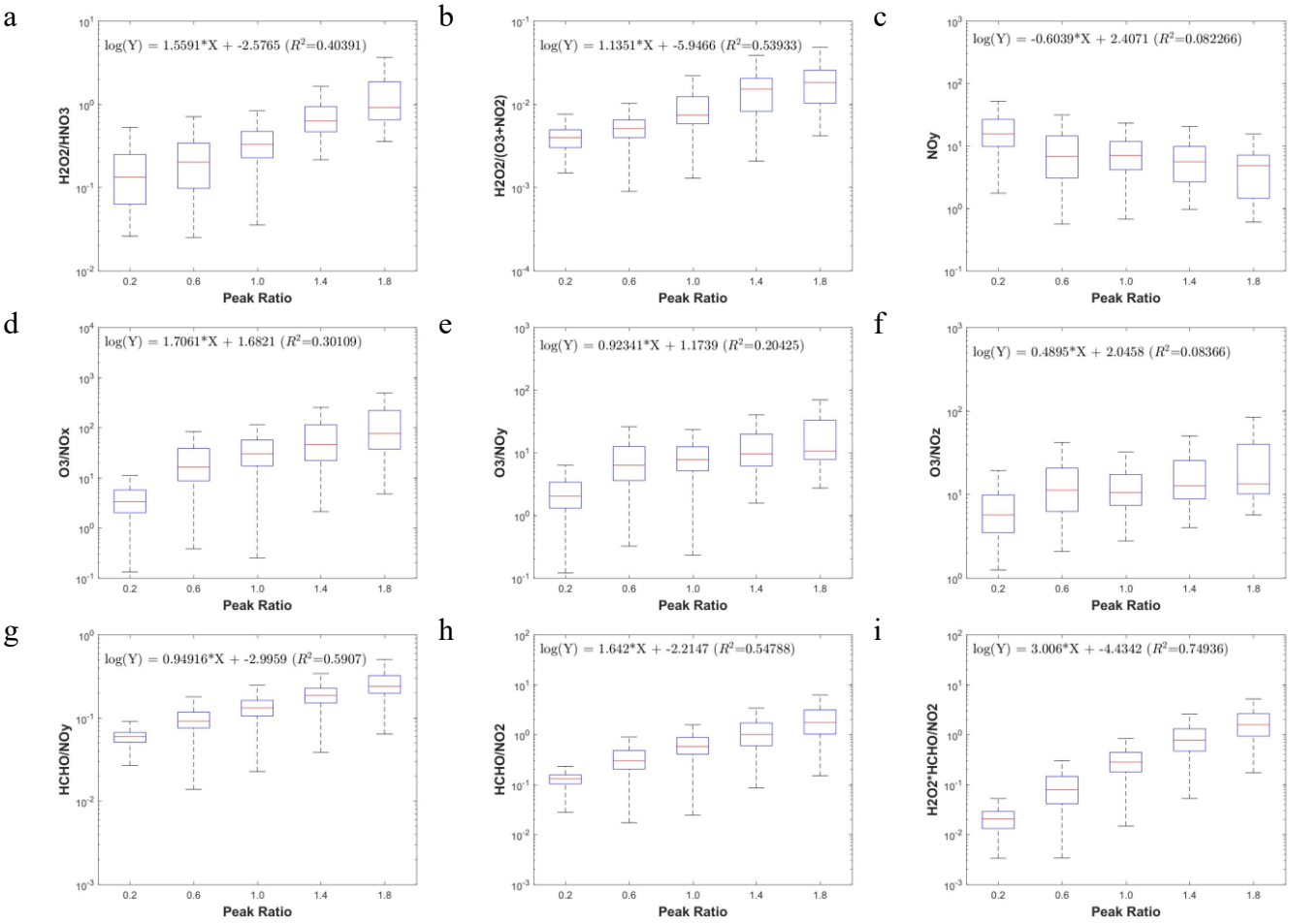

Figure 6. Development of observable responsive indicators for O_3 chemistry based on log-linear regressions between observable indicators and the PR.

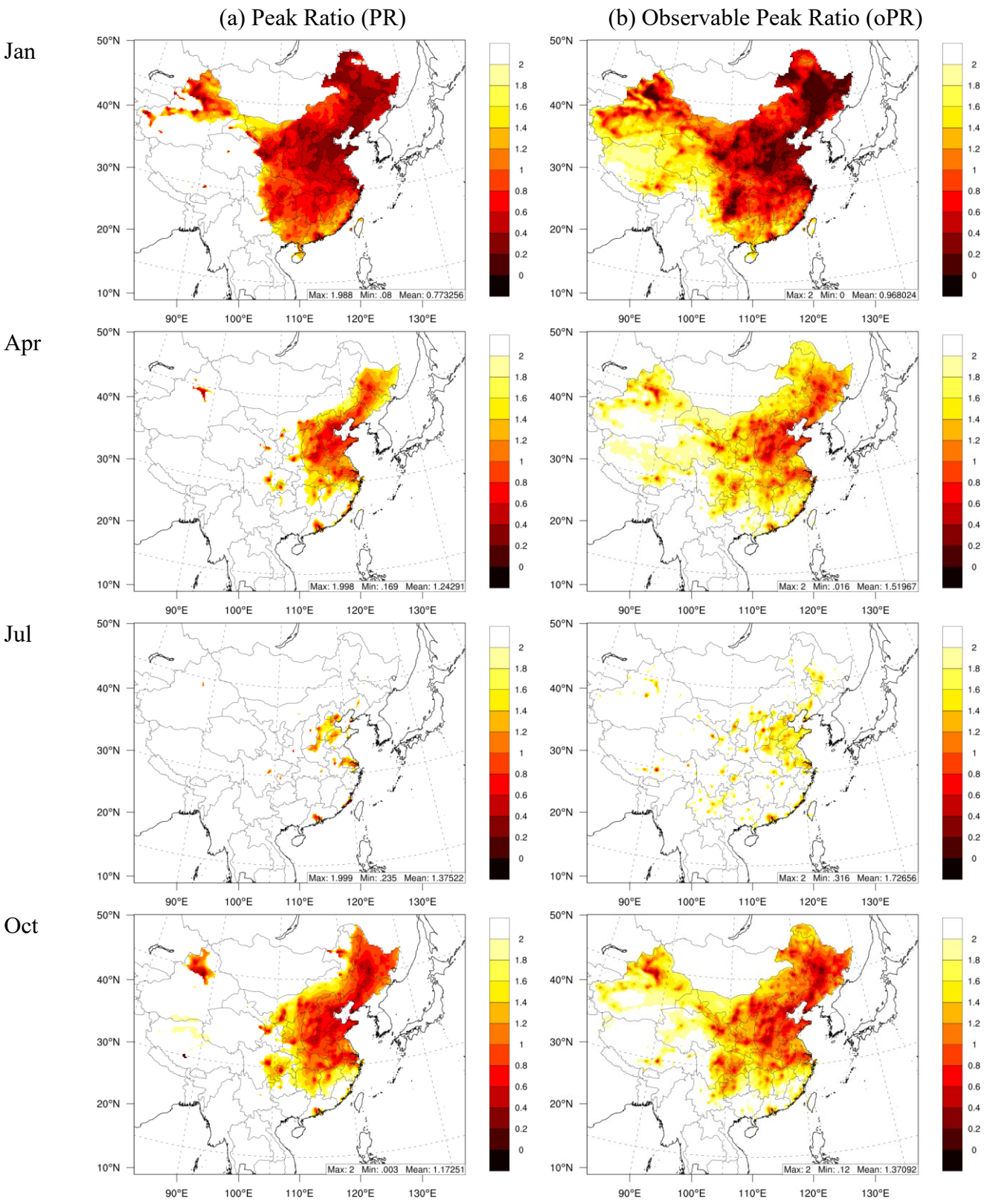

728 **Figure 7.** Comparison of the PR derived from the RSM with that calculated from concentrations for O_3
729 chemistry. The oPR was estimated based on $H_2O_2 \times HCHO/NO_2$.

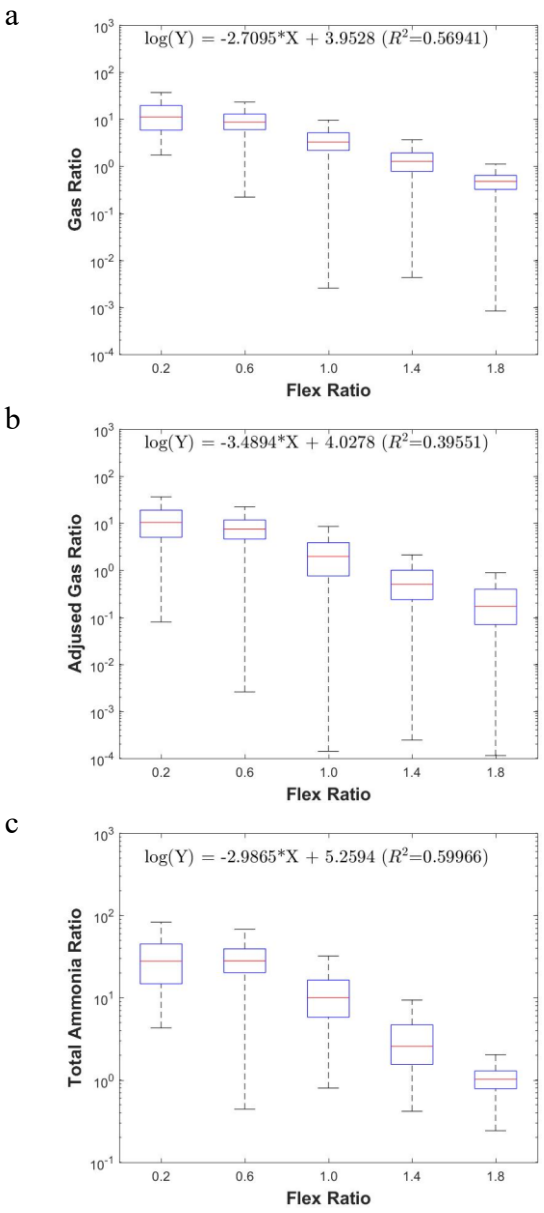

730

731 **Figure 8.** Development of observable responsive indicators for $PM_{2.5}$ chemistry based on log-linear
732 regressions between observable indicators and the FR

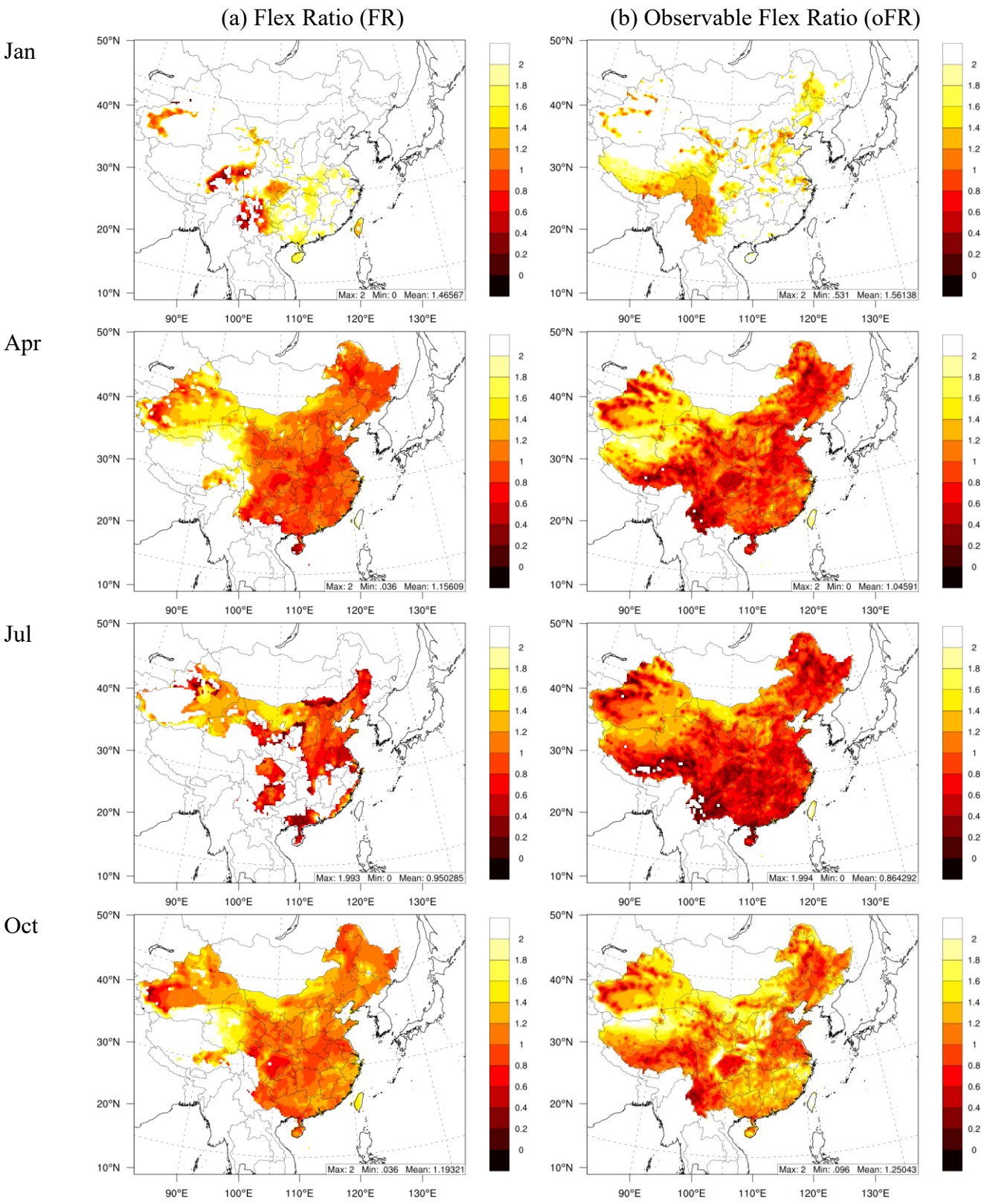

733 **Figure 9.** Comparison of the FR derived from the RSM with that calculated from concentrations for
734 $PM_{2.5}$ chemistry. The oPR was estimated based on TAR.

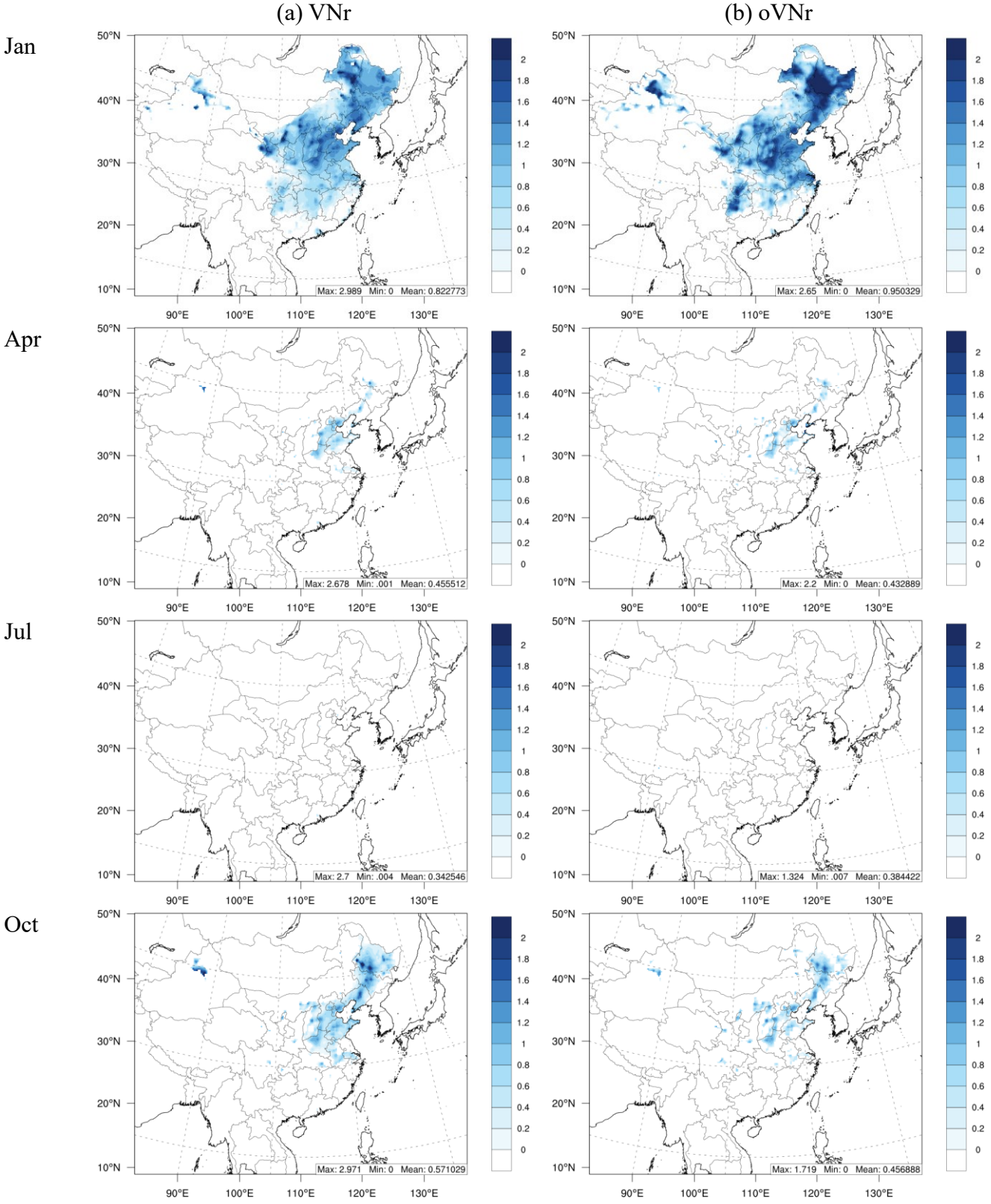

735 **Figure 10.** Comparison of VNr with oVNr.

736

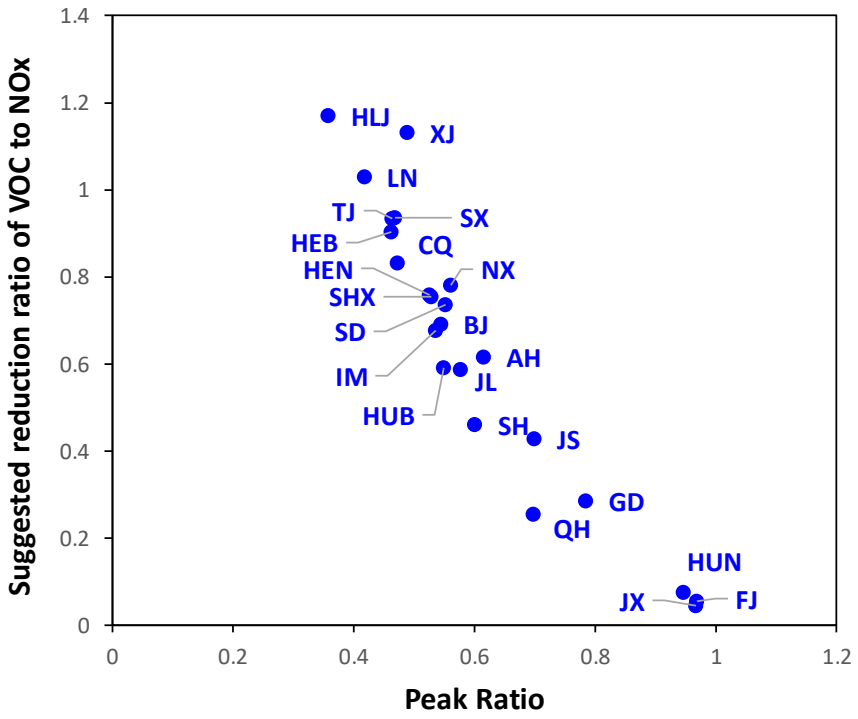

737

738 **Figure 11.** Comparison of the annual-averaged PR with VNr in each province in China

739

740

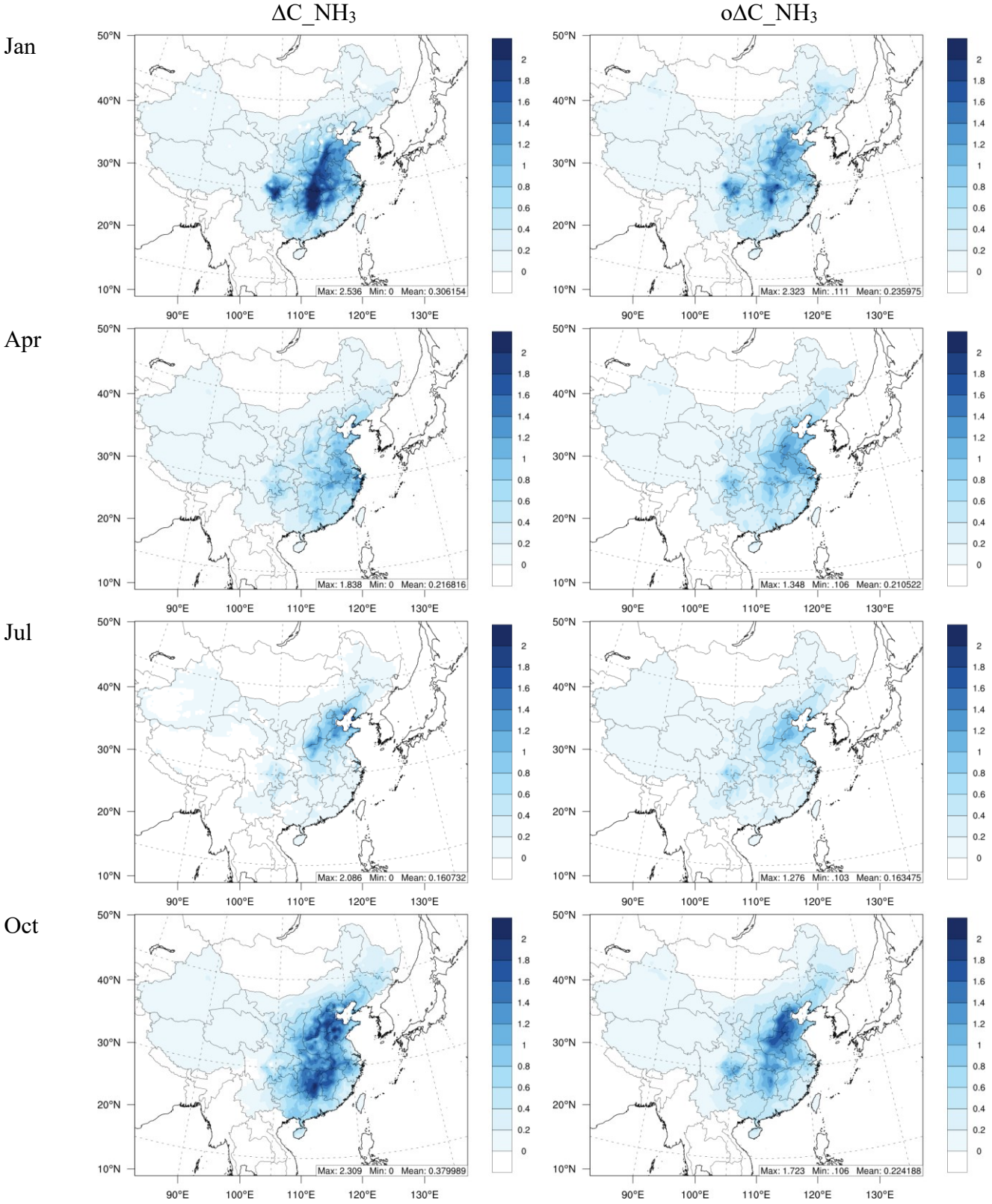

741 **Figure 12.** Comparion of the benefit in reducing $PM_{2.5}$ from simultaneous NH_3 reduction (ΔC_NH_3)
742 with that calculated from concentrations ($o\Delta C\_NH_3$)

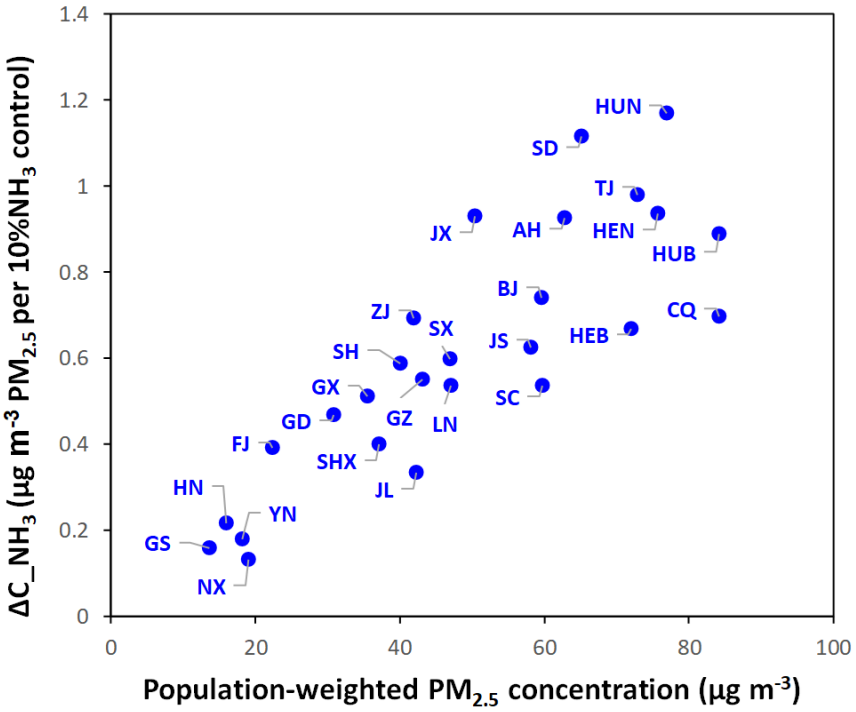

744

745 **Figure 13.** Comparison of annual-averaged benefit in reducing $PM_{2.5}$ from simultaneous NH_3 reduction
746 (ΔC_NH_3) and population-weighted $PM_{2.5}$ concentration in each province in China

747

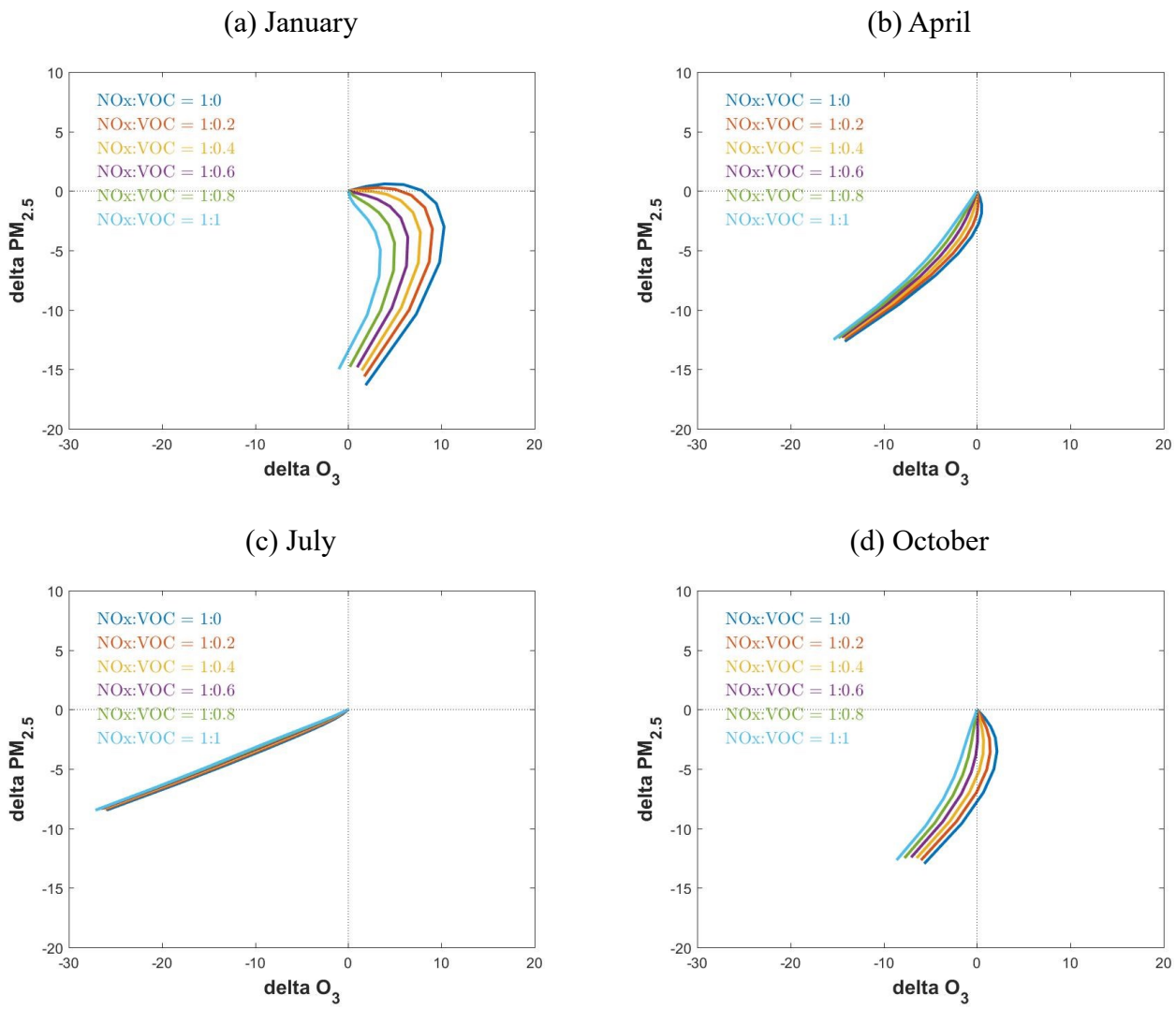

748 **Figure 14.** Control effectiveness with different NO_x and VOC ratios in reducing population-weighted
749 $PM_{2.5}$ and O_3 concentrations (in $\mu g\ m^{-3}$) in China (NO_x is from no control to 80 % reduction)